ARMY RESEARCH LABORATORY

A SURFACE ENERGY BUDGET MODEL MODIFYING HEAT FLOW BY FOLIAGE EFFECTS

David H. Tofsted

ARL-TR-60

July 1993

Approved for public release; distribution unlimited.

NOTICES

Disclaimers

The findings in this report are not to be construed as an official Department of the Army position, unless so designated by other authorized documents.

The citation of trade names and names of manufacturers in this report is not to be construed as official Government indorsement or approval of commercial products or services referenced herein.

Destruction Notice

When this document is no longer needed, destroy it by any method that will prevent disclosure of its contents or reconstruction of the document.

REPORT DOCUMENTATION PAGE

Form Approved
OMB No. 0704-0188

1. AGENCY USE ONLY (Leave blank)	2. REPORT DATE	3. REPORT TYPE AND DATES COVERED
	July 1993	Final

4. TITLE AND SUBTITLE

A SURFACE ENERGY BUDGET MODEL MODIFYING HEAT FLOW BY FOLIAGE EFFECTS

5. FUNDING NUMBERS

61102/B53A (6.1)

6. AUTHOR(S)

David H. Tofsted

7. PERFORMING ORGANIZATION NAME(S) AND ADDRESS(ES)

U.S. Army Research Laboratory
Battlefield Environment Directorate
ATTN: AMSRL-BE-M
White Sands Missile Range, NM 88002-5501

8. PERFORMING ORGANIZATION REPORT NUMBER

ARL-TR-60

9. SPONSORING/MONITORING AGENCY NAME(S) AND ADDRESS(ES)

U.S. Army Research Laboratory
2800 Powder Mill Road
Adelphi, MD 20783-1145

10. SPONSORING/MONITORING AGENCY REPORT NUMBER

11. SUPPLEMENTARY NOTES

12a. DISTRIBUTION/AVAILABILITY STATEMENT

Approved for public release; distribution unlimited.

12b. DISTRIBUTION CODE

13. ABSTRACT (Maximum 200 words)

Propagation of energy (either acoustic or electromagnetic energy) through the region of the atmosphere close to the earth's surface depends on estimates of the vertical structure of wind, pressure, temperature, humidity, and refractive index near the earth's surface. To help predict these vertical structures, the TGRAD model has been developed. The model is based on flux-profile methods, requiring simple meteorological inputs as functions of time. The model's original purpose was to predict the vertical temperature gradient profile, hence the name TGRAD. The TGRAD model has been compared against a predecessor model (the Deardorff model) and has proven to characterize the near-surface atmosphere much better under foliated conditions. It characterizes the daytime atmosphere well under all conditions studied. It characterizes the nocturnal atmosphere well until the critical Richardson number is reached. For stronger nocturnal inversions an approach is discussed that may be capable of treating these conditions. The principal improvement provided by this model is the development of sensible and latent heat flux equations that more accurately account for a surface layer partially covered by foliage.

14. SUBJECT TERMS

Boundary layer, surface energy budget, foliage sensible heat

15. NUMBER OF PAGES

86

16. PRICE CODE

17. SECURITY CLASSIFICATION OF REPORT	18. SECURITY CLASSIFICATION OF THIS PAGE	19. SECURITY CLASSIFICATION OF ABSTRACT	20. LIMITATION OF ABSTRACT
Unclassified	Unclassified	Unclassified	SAR

ACKNOWLEDGEMENT

I wish to express my appreciation to Dr. Kenneth Kunkel for his guidance throughout these investigations, for his original translation work, converting the Deardorff model into FORTRAN, and for the error analysis he performed on the TGRAD model in 1984. All of these contributed greatly to the model's present form. I also wish to thank Mr. Robert Olsen for providing the data from the Flatteville, Illinois, experiment that was used in the model verification. I'd like to also acknowledge a lot of moral support provided by Mr. Frank Hansen, who had decided not to hold his breath while waiting for this report. Finally, Dr. Henry Rachele has provided the final push to getting this manuscript moving after resting on the shelf for approximately 5 years, and Dr. Walter Bach was also helpful in reviewing the work incorporated as appendix B.

CONTENTS

LIST OF ILLUSTRATIONS 6
1. INTRODUCTION 7
1.1 History 7
1.2 Background 8
2. MODEL DISTINCTIVES AND THEORY 8
2.1 Surface Energy Budget 8
2.1.1 Controlling Variables 9
2.1.2 Introduction to Heat Flux Equations 11
2.1.3 Shortwave Radiation 12
2.1.4 Atmospheric "Longwave" Radiation Calculation 15
2.1.5 Other Terrestrial Radiative Fluxes 17
2.1.6 Convective Heat and Moisture Fluxes 18
2.1.7 Adapting Thom's Resistance Model to a Calculation of Sensible Heat . . . 20
2.1.8 Latent Heat Flux for a Foliated Layer 26
2.2 Temperature Calculations 28
2.3 Modeling Additional Air, Soil, and Plant Parameters 30
2.3.1 Moisture and Temperature Equations 31
2.3.2 Moisture Dependent Coefficients 32
2.3.3 Possible Improvements 33
2.4 Bulk Aerodynamic Parameters 34
3. SUBROUTINE DESCRIPTIONS 39
3.1 TGRAD 39
3.2 CN 49
3.3 CLOUD 50
3.4 TFOL 53
3.5 SUN 53
3.6 SPEHU 54
4. SAMPLE DRIVER 55
5. MODEL PERFORMANCE AND SENSITIVITY ANALYSIS 55
6. CONCLUSIONS 63
LITERATURE CITED 65
APPENDIX A. Calculations Involving Saturation Specific Humidity 67
APPENDIX B. Consideration of Nocturnal Temperature Gradient Structures . . . 69
DISTRIBUTION LIST 87

LIST OF ILLUSTRATIONS

TABLES

1. Symbol Table for Subroutine TGRAD 41
2. Inputs to Subroutine TGRAD 47
3. Symbol Table for Subroutine CN 50
4. Symbol Table for Subroutine CLOUD 52
5. Symbol Table for Subroutine TFOL 53
6. Symbol Table for Subroutine SUN 54
7. Symbol Table for Subroutine SPEHU 54
8. Comparison of Modeled Sensible Heats With Literature Derived Values 59

FIGURES

1. Modeled fluxes at soil surface and modeled foliage layer surface. 9
2. Foliage height H, and extrapolated zero of the windspeed profile for a fully foliated layer. 35
3. Simplified driver program TGS 56
4. Sample data set 58
5. Modeled sensible heats are compared against data measured at Deming, NM, on 14 Aug 1985, over a 15 percent foliage cover of a vineyard 60
6. Measured and modeled vertical temperature gradients for the Deming site, 14 Aug 85 60
7. Measured and modeled C_n^2 for the Deming site, 14 Aug 85 61
8. Measured and modeled C_n^2 for WSMR, NM, 15 Jul 84. The surface was nonfoliated 61
9. Comparison of measured and modeled temperature gradients for a site near Flatteville, IL, on 24 June 1984 62
10. Comparison of measured and modeled temperature gradients for the Flatteville site, on 17 Feb 1985 62

B-1. Vertical cross sections of temperature and wind relative to a turbulence cylinder. 72

B-2. Definitions of radius (r), angle (ϖ), and width (y), of a turbulence cylinder. 73

B-3. Vertical temperature gradient at 2 m above ground level as a function of time. 77

1. INTRODUCTION

For numerous years, personnel of the Battlefield Environment (BE) Directorate of the U.S. Army Research Laboratory (formerly the U.S. Army Atmospheric Sciences Laboratory (ASL) of Laboratory Command) have been actively investigating atmospheric influences on Army target acquisition systems. Among the research topics impacting target acquisition are the areas of atmospheric image distortion due to turbulence, optical refraction, acoustic propagation, scattering of acoustic waves by turbulence, and turbulence effects on laser propagation. These topics have been considered at length and continue to receive attention.

The nature of this group of problems is such that the atmosphere's vertical structure near the surface plays a critical role in the performance of Army systems. With optical refraction, the vertical structure of temperature is important. For electromagnetic energy propagation, either imaging or laser propagation, the critical parameters are the inner scale of turbulence, ℓ_o; the outer scale of turbulence, L_o; and the index of refraction structure parameter, C_n^2. C_n^2 is composed of a temperature fluctuation structure parameter (C_T^2), a related humidity term, a cross correlation term characterizing interactions between temperature and humidity fluctuations, and a pressure term.* For acoustic wave propagation the temperature, pressure, and wind vertical structures are important. For scattering of acoustic waves, the temperature (C_T^2) and wind (C_V^2) structure parameters must be considered.

1.1 History

Since these propagation problems all have the vertical structure of the near surface atmosphere in common, it would be useful to be able to predict the vertical structure of this region. Recently, H. Rachele and A. Tunick of BE have taken up this noble goal. Several papers have been produced concerning new techniques for treating sensible and latent heat flux effects on C_n^2. The applications of the Rachele/Tunick work have been in the area of turbulence effects on image propagation. Similarly, in the early 80's, K. Kunkel and D. Walters of ASL engaged in modeling the near surface atmosphere for characterization of atmospheric influences on high-energy laser propagation.

The work presented in this report was accomplished between 1982 and 1987 while the author was working on characterization of the atmosphere to predict the probability density function of atmospheric refractive effects in desert locations. The work is therefore somewhat dated, although the treatment of foliated layers is believed to be unique. It is hoped this report will provide a fixed point of reference concerning the approach taken at the time to handle the surface energy budget problem. The works of Rachele and Tunick did not exist at the time of the work, and no attempt has been made to incorporate their findings in this report. As such, for a wet environment the model presented will be less than optimal, yet for its intended purpose (refraction in deserts) the model should be appropriate.

---

*Usually the pressure term is ignored, as will be done here.

1.2 Background

The goal of a surface energy budget model is to simulate the heat fluxes at the earth's surface and, in so doing, to recreate the environment wherein the vertical structures of the atmosphere exist. This approach assumes that there exist specific linkages between the fluxes at the surface and the vertical structures. This linkage is handled through similarity theory and the flux-profile relationships.

Since Halstead *et al.* (1957) developed an analog computer to simulate the surface energy budget, many authors have attempted to derive equations that accurately calculate turbulent heat fluxes in the surface layer. When this research is coupled to flux-profile theory (Dyer, 1974), atmospheric structure profile predictions for near-surface conditions are possible.

2. MODEL DISTINCTIVES AND THEORY

In general, the theory discussed here deals with the basic equations necessary to calculate the surface layer aerodynamic parameters of friction velocity, u_*, Obukhov length, L (Obukhov, 1946), soil temperature, and foliage temperature. Once these parameters are known, only a single step is needed to produce complete estimates of the vertical structures mentioned in section 1. To compute u_* and L, the sensible heat flux, H_{Sh}, must first be found. To find the sensible heat flux, the force-restore surface energy budget method is used. This method is simultaneously coupled with an iterative Obukhov length calculation.

2.1 Surface Energy Budget

The surface energy budget approach developed here is based on Deardorff's (1978) model that included vegetation layer effects. This model had been programmed in FORTRAN by K. Kunkel of ASL prior to the time the author began work on the model. The Deardorff model calculates the radiative, convective, and conductive energy fluxes from a ground surface layer and a foliage layer. Here the use of the term foliage layer refers to an equivalent surface of plants that obstructs the transit of radiation flowing from the atmosphere to the earth. The mean height of this layer is variable, as well as the overall fraction of the ground surface covered. The fractional foliage coverage is denoted by the term σ_f and represents that fraction of the surface that intercepts/blocks direct sunlight from reaching the ground. In this model the foliage layer can be thought of as a low lying layer of weeds, grass, or bushes.

The fluxes to and from the surface may be divided between those above the foliated layer (denoted by h), fluxes between the foliage and the surface (denoted by g), and the

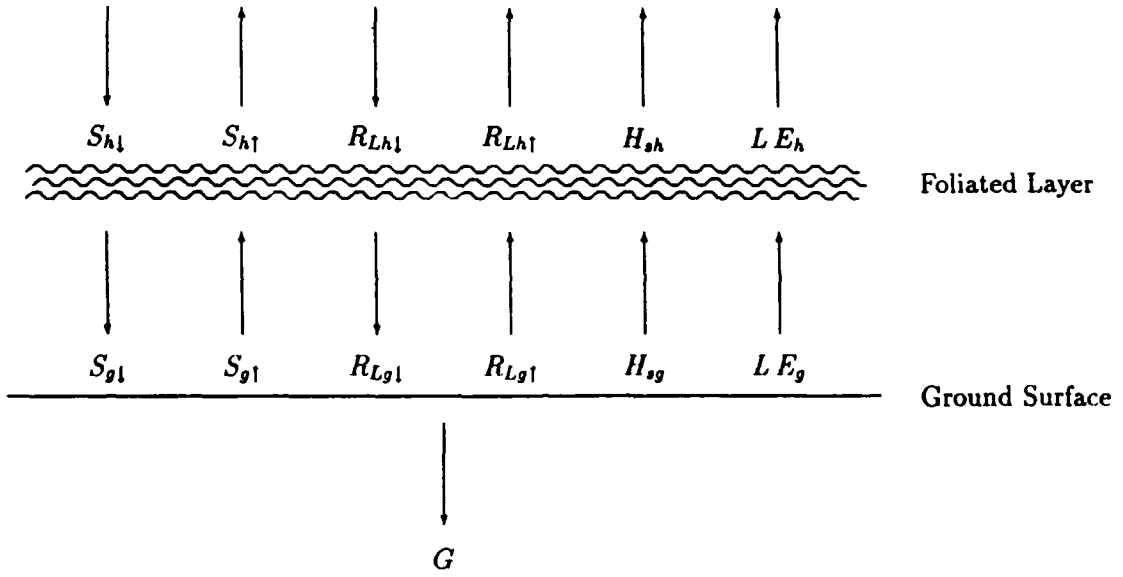

Figure 1. Modeled fluxes at soil surface and modeled foliage layer surface.

conductive heat flux into the soil (denoted by G). Figure 1 shows the directionality of the fluxes involved.

The fluxes are further divided by the type of energy being transported. There are shortwave (S) and longwave (R_L) radiative fluxes,* convective fluxes in latent form (due to evaporation or condensation) (L_vE) and in "sensible" form (due to warming or cooling of air at the surface) (H_S), and the conductive flux (G) of heat into the soil. Radiative fluxes can be directed either upward or downward, while sensible and latent heats are only handled by single functions (having positive senses when the fluxes are directed away from the surface).

2.1.1 Controlling Variables

Excluding the shortwave fluxes, the remaining fluxes depend on one wind, six temperature, and four humidity variables. Time variations in these variables to a great degree determine the behavior of the vertical structures to be predicted. The wind variable, u, is a measured

---

*Shortwave usually refers to all radiation at wavelengths shorter than 4 μm. Longwave refers to all radiation at wavelengths longer than 4 μm. The separation occurs naturally since solar radiation is negligible at wavelengths greater than 4 μm, while terrestrial (graybody) radiation has negligible contributions at wavelengths below 4 μm. (See Oke (1978), page 11.)

input to the model. It is measured at a model input reference height, z_s. The first five of the temperature variables are θ_g, the temperature of the ground at the surface; θ_2, the temperature of the ground a characteristic distance below the surface, where this distance is dependent on soil type; θ_f, the foliage temperature; θ_a, the measured air temperature at the reference height; and θ'_a, a simulated air layer temperature at the reference height that is driven by the surface heat fluxes and a restoring term based on θ_a.*

The ground temperature is modeled as a function of the driving energy fluxes at the surface, as modulated by what Hoffert and Storch (1979) call the thermal inertia of the ground. The thermal inertia depends on the depth (d_1) to which the thermal wave can penetrate the soil in a day. This penetration depth is modeled as

$$d_1 = \sqrt{\kappa_s \tau_{day}}, \tag{1}$$

where κ_s is the soil's thermal diffusivity in $m^2 s^{-1}$, and τ_{day} is the number of seconds in a day (86400 s). The deep ground temperature θ_2 is modeled as controlled by the depth of penetration of the thermal wave on a yearly basis ($d_2 = \sqrt{365}\, d_1 = 19.1\, d_1$).

The sixth temperature variable is the upper-air temperature (θ_{ua}), which is used in the estimation of the downward longwave sky radiation from clouds. The value of θ_{ua} is based on the measured air temperature and the type of clouds present. A simple estimation scheme is used: for low clouds $\theta_{ua} \approx \theta_a - 8$, for medium clouds $\theta_{ua} \approx \theta_a - 16$, and for high clouds $\theta_{ua} \approx \theta_a - 24$. The predictions are based on assumed heights of cloud bases of about 1200, 2400, and 3600 m, respectively, using a 6.5 K/km temperature lapse rate (the moist adiabatic lapse rate).

The 4 humidity variables used in the model are the atmospheric relative humidity measured at the station height (R_H), the amount of dew (in kg/m^2) on the foliage (w_{dew}), and the fractional water contents (by volume) within the first 10 cm of soil (w_g) and within the first 50 cm of soil (w_2). The distances 10 cm and 50 cm roughly equate to the depths of soil affected by the daily (d_1) and yearly (d_2) variation of temperature. Thus the soil characteristics in the layer nearest the surface will be characterized by θ_g and w_g. Similarly, θ_2 and w_2 will be associated with the deeper layer. The importance of this association is made clear in section 2.3 when the equations for soil thermal characteristics, which depend on the moisture content, are discussed.

Below the depth of 50 cm, the model assumes the ground has no fluctuations in temperature. Oke (1978) shows a yearly peak-to-peak thermal wave amplitude of approximately

---

*In all equations hereafter θ'_a will be replaced by θ_z, which is considered descriptive of the air temperature at height z_s. In general θ_z will not equal the measured air temperature since it is assumed the surface temperature controls the variation of air temperature near the surface rather than air temperature driving surface temperature variations. θ_z is the means of handling this driving mechanism. A combination of surface flux driven temperature variations and a stabilizing term allow the model to pace the behavior of the near surface atmosphere. The stabilizing term, moreover, avoids the model phenomenon of surface temperature "creep" that often plagues long term prediction models. This change was effected after Kunkel's (1985) review of the model and upon his suggestion.

10 K at 1 m below the surface. Thus the approximation used in the model could be improved, though it is unlikely to strongly affect behavior of atmospheric structure predictions since the heat exchange with the soil below 50 cm is small in comparison to the radiative and convective fluxes at the surface.

2.1.2 Introduction to Heat Flux Equations

The temperatures θ_g and θ_f can be found as a function of time by solving the surface energy budget equations. The equation for the surface energy budget at the foliated layer can, in fact, be cast as a direct function of the foliage temperature. Therefore solution of one of the energy budget equations allows direct estimation of one of the temperature parameters of interest.

Since the foliated layer's ability to store heat is assumed negligibly small, the fluxes arriving at the foliage layer from above and below must sum to zero. From figure 1 this sum can be expressed as

$$\begin{aligned} S_{h_\downarrow} + S_{g_\uparrow} + R_{Lh_\downarrow} + R_{Lg_\uparrow} + H_{Sg} + LE_g = \\ S_{h_\uparrow} + S_{g_\downarrow} + R_{Lh_\uparrow} + R_{Lg_\downarrow} + H_{Sh} + LE_h. \end{aligned} \tag{2}$$

The foliage temperature is found by means of a Newton-Raphson method (see section 2.2), where the foliage temperature defines a unique solution to equation (2).

The condition that makes the calculation of energy fluxes at the foliated layer critically important is precisely because the foliage surface has no thermal inertia and because the leaves have more surface area than the ground below. That is, while the fraction of direct sunlight blocked by the leaves rarely exceeds 70 percent (Deardorff, 1978), the exposed leaf surface area (available for evapotranspiration and sensible heat exchange) is about seven times the surface area of terrain overshadowed. Thus a fully vegetated surface can be much more of an influence on the convective fluxes of momentum, sensible heat, and latent heat than the underlying surface. Foliated layer effects therefore have a significant impact on atmospheric structure predictions, which will alter propagation model results, which will in turn influence system performance under those atmospheric conditions. To properly model foliage effects, a surface energy budget model was modified by Deardorff to account for the interactions at the foliated layer.

The other key temperature to be predicted is the soil surface temperature. To predict this temperature as a function of time requires a different method from that used to compute foliage temperature because of the thermal inertia of the ground. Here, heat is conducted into and stored in the soil as well as being exchanged in fluxes above the surface. These storage terms make the Newton-Raphson method inappropriate.

The amount of energy in the soil as a whole is characterized by the variable θ_2. Yet it is only the soil's temperature at the surface (θ_g) that is involved in equations describing energy fluxes to the atmosphere above. Thus two equations are required, one describing the energy fluxes at the surface, which are necessarily in balance,

$$G = S_{g_\downarrow} - S_{g_\uparrow} + R_{Lg_\downarrow} - R_{Lg_\uparrow} - H_{Sg} - LE_g, \tag{3}$$

and a second equation describing the actual ground surface temperature change,

$$\frac{\partial \theta_g}{\partial t} = \frac{c_1 G}{I_1} + \frac{c_2(\theta_2 - \theta_g)}{\tau_{day}}. \tag{4}$$

This is called the force-restore method, based on the theories of Bhumralkar (1975) and Blackadar (1976). Blackadar used the values $c_1 = 3.72$ and $c_2 = 7.4$ for the transfer coefficients, and I_1 is Hoffert and Storch's (1979) thermal inertia

$$I_1 = \rho_s c_s d_1, \tag{5}$$

where ρ_s is the soil density and c_s is the soil's specific heat. (Together, the quantity $\rho_s c_s$ is the soil heat capacity.)

Though θ_2 is approximately constant over the span of a few days, when modeling long time spans it must be calculated by the equation

$$\frac{\partial \theta_2}{\partial t} = \frac{G}{I_2}, \qquad I_2 = \rho_s c_s d_2, \qquad d_2 = \sqrt{365\,\tau_{day}\kappa_s}. \tag{6}$$

To model the annual trend of the deep soil temperature, R. Johnson (then of ASL) developed the following approximation to be used to initialize θ_2 for desert environmental conditions:

$$\theta_2 \approx 291.66 + 9 \sin\left(360\frac{(J_D - 130)}{365}\right),$$

where θ_2 is the temperature given in degrees Kelvin and J_D is the Julian date. When the Johnson approximation is used, model behavior of the G flux will rapidly approach realistic values since there will not be transfer of energy between the deep soil and the near surface soil with the *wrong sign* for that time of year (when considering a desert environment at approximately 30° N latitude). Approximations similar to the Johnson equation could be developed for other environments as well.

2.1.3 Shortwave Radiation

Each of the flux terms in equations (2) and (3) will now be considered in explicit form. The first to be considered is the shortwave radiation from the sky, $S_{h_\downarrow}$. This flux depends on the solar zenith angle and the amount of cloud cover. The amount of cloud cover (C_C) must be input to the model. This input is normally accepted for a single layer, but provisions in the model allow for input of separate skycover fractions at low, medium, and high cloud heights utilizing the cloud model of Shapiro (1982).

One of the key aspects of any radiation model is to locate the sun within the sky. Several additional model inputs and calculations are required to compute the solar zenith angle. In subroutine `SUN` the solar zenith is computed from a knowledge of local standard time, latitude, longitude, and day of the year. The following procedure is used:

The time of local noon is given in minutes after midnight as

$$\Xi = 720 - \epsilon_T + 4\Delta_\Lambda, \tag{7}$$

where ϵ_T is the equation of time (Smithsonian Meteorological Tables, 1951) approximated by (Woolf, 1968)

$$\epsilon_T = -60 \left(\frac{\sin(A)}{8.09258} - \frac{\cos(A)}{233.155} + \frac{\sin(2A)}{6.50157} - \frac{\cos(2A)}{16.45278} \right), \tag{8a}$$

with

$$A = (J_D - 1)\,\frac{360}{365.242}, \tag{8b}$$

where all arguments to trigonometric functions are given in degrees.

The quantity $720 - \epsilon_T$ computes the time of solar noon, but only for locations at standard meridians (Λ_{stdm}). The Δ_Λ term in equation (7) is the means of correcting for solar noon at a local longitude. Assuming east longitudes are treated as negative and west longitudes as positive, Δ_Λ is defined as

$$\Delta_\Lambda = \Lambda_{local} - \Lambda_{stdm}, \tag{9}$$

where Λ_{local} is the local longitude in degrees.

Using this convention, anytime a location is west of the standard meridian used to measure clock hours, the time of solar noon will be 4 minutes later per degree of difference between the local longitude and the standard meridian. Normally this correction will be small, but for some time zones it may be up to an hour's difference.

The second quantity to be calculated by the SUN subroutine is the solar declination, D_S. A formulation based on Woolf (1968) is used.

$$D_S = \sin^{-1}(\sin(23.4438)\,\sin(\delta)), \tag{10a}$$

$$\delta = A + 279.9348 + 1.914827\,\sin(A) - \frac{\cos(A)}{12.5747} + \frac{\sin(2A)}{50.1555} - \frac{\cos(2A)}{617.284}, \tag{10b}$$

where all arguments to the trigonometric functions are assumed measured in degrees.*

Declination is considered constant over the course of a single Julian date.

The SUN routine then computes H_d, the fraction of the day between sunrise and local noon. By calculating this quantity, sunrise and sunset times can be determined about the local noon.

$$\cos(2\,\pi\,H_d) = \left(\frac{\sin\beta - \sin\ell\,\sin D_S}{\cos\ell\,\cos D_S} \right), \tag{11}$$

---

*Appropriate conversions to radians will be required for some compilers.

where ℓ is the local latitude, and β (equal to -50 minutes of arc) is the elevation angle when sunrise occurs (β is nonzero due to astronomical refraction effects). Sunrise and sunset times (in minutes from midnight) are then

$$I_{sunrs} = \Xi - 1440\, H_d, \tag{12a}$$

$$I_{sunst} = \Xi + 1440\, H_d. \tag{12b}$$

Given the declination, sunrise and sunset times, and the local time in minutes past midnight, one can compute the solar energy flux reaching the top of the earth's atmosphere using a plane parallel assumption. Subroutine CLOUD is called to make this calculation.

Within subroutine CLOUD (based on Shapiro (1982)), reflections between cloud layers are treated. First, the solar radiation is calculated from the average solar radiation intensity at the earth's mean orbit radius ($S_{0(mean)}$=1353 W/m^2) and is corrected by factors accounting for the actual distance to the sun. This value is then adjusted according to the cosine of the zenith angle, the effective surface albedo, and the cloud type and cloud amounts in three cloud layers.

Mathematically, this process is described in the following equations. The actual solar irradiance at the earth's distance from the sun is determined by accounting for the distance variations of the earth from the sun as a function of day of the year through the equation

$$S_0 = S_{0(mean)} \left(\frac{\overline{Dist}}{Dist} \right)^2, \tag{13a}$$

where $\overline{Dist}/Dist$ represents the ratio of the average to the actual distance to the sun:

$$\frac{\overline{Dist}}{Dist} = \left(1.00014 + 0.016726 \cos\left(\frac{360\,(J_D - 2)}{365} \right) \right). \tag{13b}$$

The irradiance at a plane perpendicular to the earth-sun axis must now be translated into the energy entering a plane parallel atmosphere through use of the cosine of the zenith angle. The cosine of the zenith angle ($\cos\zeta$) is determined from the latitude (ℓ), declination (D_S), and hour angle (H_r) as

$$\cos\zeta = \sin\ell \sin D_S + \cos\ell \cos D_S \cos H_r, \tag{14}$$

where time t in minutes past midnight is converted into an angle through $H_r = 360\,t/1440$. Thus

$$S_1 = S_0 \cos\zeta$$

is the energy flux from the sun (in W/m^2) at the top of the atmosphere.

This flux is propagated to the surface where a portion of it is absorbed. The absorbed portion is $(1 - \alpha_e)$, where α_e is the effective albedo of the surface. The effective albedo is the average reflectivity of the surface. This factor considers the fractional reflectance

from that portion of the surface covered by foliage (σ_f) and reflection from the fractional exposed surface area ($1 - \sigma_f$):

$$\alpha_e = \sigma_f \alpha_f + (1 - \sigma_f)^2 \alpha_g A_{\infty(s)}, \tag{15a}$$

$$A_{\infty(s)} = (1 - \alpha_g \alpha_f \sigma_f)^{-1}, \tag{15b}$$

where α_f is the mean shortwave reflectivity (albedo) of the foliage, and α_g is the albedo of the soil. The effective albedo is thus composed of a component representing reflection from the foliage plus a component representing that portion of the incident energy that passes through the foliage layer, reflects off the surface, and passes back through the foliage layer. The factor $A_{\infty(s)}$ represents the effects of contributions from multiple reflections between the foliage layer and the surface before the energy escapes into the upward flux above the layer.*

In the CLOUD subroutine, a complicated series of reflection and transmission calculations between different cloud layers and the surface is made. Shapiro (1982) gives a fuller explanation of this procedure. Here it will be expressed simply as

$$S_{h_\downarrow} = S_0 \chi \cos\zeta, \tag{16}$$

where χ represents the fractional attenuation of sunlight due to the cloud filled atmosphere.

2.1.4 Atmospheric "Longwave" Radiation Calculation

As previously explained, atmospheric radiation is characterized by infrared emissions from atmospheric constituents.† In this model the downward longwave flux from the atmosphere is parameterized using the equation

$$R_{Lh_\downarrow} = \epsilon_a \sigma \theta_a^4 + (1 - \epsilon_{ua}) C_{Ct} \sigma T_{ua}^4, \tag{17}$$

accounting for near-surface molecular emissions and emissions from clouds. In this equation ϵ_a is the average emissivity over the infrared spectrum of the air near the surface (thus distinguishing it from blackbody radiation where the emissivity is unity).

The cloud layer contribution to the longwave flux is characterized by the second term on the right in equation (17). The emissivity of the cloud layer is assumed to be unity. C_{Ct} is the total fractional portion of the sky covered by clouds (where all the clouds are assumed

---

*$A_{\infty(s)}$ is found as the solution to the infinite series $1 + x + x^2 + ... = (1 - x)^{-1}$, where $x = \alpha_g \alpha_f \sigma_f$ is that portion of the energy trapped between the foliage and surface that survives a round trip of reflection at the surface and at the foliage layer.

†Since these emissions only approximate a perfect blackbody spectral shape, they are often called graybody radiation. Gaseous emitters have gaps in their emission spectra, called windows, where no emission bands exist. Solid surfaces have smoother emission spectra, but emit at slightly below 100 percent efficiency.

to be incorporated into a single parameter at a single height). As previously discussed, the temperature of the upper air (cloud temperature, T_{ua}) is used to characterize the longwave emissions source region. The assignment of a temperature value to this region is a "best guess."*

The σ used in equation (17) is the Stefan-Boltzmann constant (equal to 5.67×10^{-8} W/(m^2 K^4)).

Note that the cloud temperature is represented using a T variable rather than a θ variable. The T variables will always be used for temperatures, while the θ variables will always be used for potential temperatures. The two are related through the equation

$$\theta = T - \Gamma z,$$

where z is the height above the ground and Γ is the adiabatic lapse rate (-9.8 K/km in dry atmospheres, -6.5 K/km in moist atmospheres). For a neutrally stable (adiabatic) atmosphere, θ would be constant with height while T would decrease at the rate of Γ. Since most atmospheric structure models are dependent on the stability, $d\theta/dz$ is much more important than dT/dz, and thus θ is a more natural choice for the temperature variable near the surface than T. But, when radiant emissions are considered, the amount of radiant energy depends on T not θ. Because Γ is small, assuming measured air temperature T_a is approximately equal to θ_a represents minimal error so long as the station height z_s is within a few meters of the ground. However, for the longwave emissions from clouds, the parameter T_{ua} must be used.

The atmospheric emissivity (ϵ_a) used in equation (17) has been parameterized by Deardorff (1978) using the theory by Staley and Jurica (1972). In the present model a slightly modified version of the Deardorff equation is used:

$$\epsilon_a = 0.67\, e^{0.08}\,(1.52 - 0.0018\,\theta_a), \tag{18}$$

where e is the atmospheric vapor pressure at the station height in millibars.

The deviation of equation (18) from that of Deardorff is the term linear in θ_a, which modifies the emissivity based on temperature. The rationale for this modification is that the atmosphere contains two *window* regions at 3-5 μm and 8-12 μm in the infrared. Otherwise, the atmosphere is nearly opaque. If one therefore assumes that the atmosphere is emitting energy as a blackbody at all wavelengths except those in the two window regions and that no emissions in the window regions occur, then one can compute the fraction of energy emitted (absorbed) by such a graybody at a given temperature. Performing this task, one finds that at 288 K the emissivity of such a graybody is 0.74, or a result very similar to the modeled result of Staley and Jurica. This tends to indicate the physics of the approach described is encompassing the essentials of the emission process being modeled by the original equation. Upon performing the calculation at a series of other

---

*Also notice that the air temperature θ_a used in the longwave flux calculation is based on the input air temperature rather than the computed temperature, θ_z. This keeps the downward longwave heat flux from contributing to any temperature creep effects.

temperatures, one obtains a curve that exhibits a nearly linear trend with temperature. This trend is given by the correction term in equation (17).

Interestingly, the slope of the correction is negative since with increasing temperature a greater fraction of the radiant energy would be emitted from the window regions (if the windows were radiatively active). Since the windows are not radiatively active, the effective emissivity decreases. The choice of coefficients 1.52 and 0.0018 is such that the correction term equals 1 when $\theta_a = 288$ K (or for a standard atmospheric temperature similar to that under which the results of Staley and Jurica would have been obtained). At higher temperatures, eventually the effective emissivity rises once more, but the temperature at which this occurs is far above those normally encountered on earth, and thus the linear trend is all that is necessary.

The sky emissions have therefore been divided into two segments. In the first segment, the near surface air temperature is used to describe emissions from air near the surface at wavelengths **outside** the atmospheric window regions. In the second segment, the clouds are treated as blackbody surfaces at the upper air temperature. The energy arriving from the clouds is treated as proportional to the fraction of the sky covered by clouds and as proportional to that portion of the energy emitted by the clouds that is **in** the window region of the spectrum and would not be absorbed by the intervening air on its way to the surface. The calculation of ϵ_{ua} is therefore the same as equation (18), except that T_{ua} replaces θ_a since the spectrum of energy depends on the cloud temperature and not the near-surface air temperature.

2.1.5 Other Terrestrial Radiative Fluxes

The remaining radiative fluxes originate due to reflective and emissive properties of the foliage (f) and ground (g) surfaces. To represent these quantities, Deardorff used α_g and α_f for the mean albedos of the ground and foliage surfaces, respectively, at visible wavelengths. ϵ_g and ϵ_f were assigned the average longwave radiative emissivities for ground and foliage (see Deardorff (1978) or Oke (1978) for tables of typical values). (Thus the quantities $(1-\epsilon_g)$ and $(1-\epsilon_f)$ represent the longwave reflectivity coefficients for the ground and foliage.)

From these quantities Deardorff estimated the remaining six radiative fluxes in equations (2) and (3). Equations (19) and (20) are similar to the equations Deardorff used for the shortwave and longwave fluxes.

$$S_{g\downarrow} = (1-\sigma_f)\, S_{h\downarrow}\, A_{\infty(s)}, \tag{19a}$$

$$S_{g\uparrow} = \alpha_g\, S_{g\downarrow}, \tag{19b}$$

$$S_{h\uparrow} = (1-\sigma_f)\, S_{g\uparrow} + \sigma_f\, \alpha_f\, S_{h\downarrow} = \alpha_e\, S_{h\downarrow}, \tag{19c}$$

$$\begin{aligned} R_{Lg\downarrow} &= (1-\sigma_f)\, R_{Lh\downarrow}\, A_{\infty(\ell)} \\ &\quad + \sigma_f\, [\epsilon_f\, \sigma\, \theta_f^4 + (1-\epsilon_f)\, \epsilon_g\, \sigma\, \theta_g^4]\, A_{\infty(\ell)}, \end{aligned} \tag{20a}$$

$$R_{Lg\uparrow} = (1-\sigma_f)\, [\epsilon_g\, \sigma\, \theta_g^4 + (1-\epsilon_g)\, R_{Lh\downarrow}]\, A_{\infty(\ell)} \tag{20b}$$

$$+\sigma_f\left[\epsilon_g\,\sigma\,\theta_g^4+(1-\epsilon_g)\,\epsilon_f\,\sigma\,\theta_f^4\right]A_{\infty(\ell)},$$

$$R_{Lh_\uparrow}=(1-\sigma_f)\left\{\epsilon_g\,\sigma\,\theta_g^4+(1-\epsilon_g)\left[(1-\sigma_f)\,R_{Lh_\downarrow}+\sigma_f\,\epsilon_f\,\sigma\,\theta_f^4\right]\right\}A_{\infty(\ell)} \qquad (20c)$$
$$+\sigma_f\left\{\epsilon_f\,\sigma\,\theta_f^4+(1-\epsilon_f)\,R_{Lh_\downarrow}\right\},$$

$$A_{\infty(\ell)}=(1-(1-\epsilon_f)(1-\epsilon_g)\,\sigma_f)^{-1}. \qquad (20d)$$

Note that in equation (19a) the amount of energy reaching the surface is the fraction of direct energy passing through the foliated layer multiplied by the factor $A_{\infty(s)}$. The factor $A_{\infty(s)}$ was introduced in equation (15b). Likewise, $A_{\infty(\ell)}$ represents the effects of multiple reflections in the infrared. The main assumption made here is that the vegetation layer can be effectively replaced by a partially opaque plane surface. Actually, this type vegetation layer will never exist, but mathematically it allows for a simple calculation of the multiple reflections. The Deardorff model assumes that only single scattering occurs. Equations (19) and (20) are thus a small improvement on the Deardorff model. Note, however, that normally $A_{\infty(s)}$ will be close to unity, so that Deardorff's original equations obtain nearly the same results.

2.1.6 Convective Heat and Moisture Fluxes

The fluxes of sensible and latent heat are driven by the bouyant and forced mixing of a spectrum of different sized turbulent air elements close to the ground. The general term of "eddy" is used to describe these elements. Many simplified models have been used to calculate these fluxes, of which Deardorff's model is typical. These models are called simplified because a fixed value is used for the heat exchange coefficient during all unstable (daytime) cases and a second fixed quantity for all stable (nighttime) cases. However, the Deardorff model also considered the incorporation of a foliated layer, and this aspect of his model (suitably modified) has been transitioned to the model discussed here.

To model the vegetation layer, Deardorff used a modified air temperature, vapor pressure, and windspeed that were to be characteristic of the values of these parameters in the vicinity of the leaves of the vegetation. While some other aspects of the Deardorff approach will be retained, this particular aspect (of using near leaf parameters) will be modified because it leads to overprediction of sensible heat for highly foliated surfaces.

A second (and somewhat better) method for calculating the sensible and latent heat fluxes is through the flux-profile technique employed by Hoffert and Storch (1979) for nonvegetated surfaces. Once the Hoffert and Storch model for sensible heat flux is suitably modified for foliated surface effects, constant flux coefficients are unnecessary since the method develops its own coefficient values dynamically, based on the current atmospheric stability.

The basis of the modified approach detailed here is the flux-profile method. The flux-profile method uses scaling parameters that characterize the current atmospheric state within the surface layer (Dyer, 1974). The scaling parameters are obtained through flux-profile relationships. These parameters can then be related to vertical profile shapes, based

on the similarity theory of Obukhov (1946). Using this technique, the sensible heat flux (H_{Sh}) is determined by the equation

$$H_{Sh} = -\rho C_P T_* u_*, \tag{21}$$

where ρ is the dry air density, C_P is the specific heat of dry air at constant pressure, T_* is the scaling temperature (Hoffert and Storch, 1979), and u_* is the friction velocity.

Using this equation for sensible heat flux is a departure from the Deardorff method, which uses an equation similar to that outlined by Priestley (1959, see pp. 4-6 and 39-43).*

The justification behind the search for a more satisfying calculation for sensible heat can be traced back to the initial purpose of the model. Originally, the author was looking into the atmospheric refraction problem. In this problem the dominating factor influencing the daytime vertical temperature profile is the sensible heat flux H_{Sh}. Errors in the estimation of H_{Sh} would therefore immediately be translated into errors in estimation of the temperature structure. Initial model experimentation using Deardorff's method showed sensible heat fluxes up to 700 W/m^2 for heavily foliated conditions. These high values were considered erroneous and found to be the result of using an inflated value for sensible heat flux flow coefficient, K_H, when σ_f was large. The justification used by Deardorff to explain the increase was that the exposed surface area for sensible heat flux exchange was increasing directly as the fractional foliage cover increased. Thus the reasoning followed that higher fluxes would result from a higher exposed surface area.

The problem with this logic is that the sensible heat, according to flux-profile theory, depends only on the shapes of the vertical profiles of temperature and windspeed, not on the exposed area near the surface. Flux-profile theory thus predicts that there is a saturation effect on the carrying capacity of the air that is passing through the foliated layer and next to the surface. The air must travel close enough to the leaves, stems, and ground surface to transfer energy and then must be replaced by new air from above that has not yet been influenced by the surface elements. But the air near the surface cannot be immediately replaced by air from above. Thus some portions of the plant and soil surfaces will always be in contact with air that has become partially adjusted to the warmer (or cooler) temperature. Deardorff tried to consider this aspect by parameterizing temperatures very close to the surface and leaves, but his attempt was only partially successful. In fact the more foliage present, the more of a barrier will exist to restrict the free flow of air into the vegetated canopy, and the greater effect the drag of the foliage will have on the overall windflow patterns near the surface.

Despite this limitation, the Deardorff model documented the increased efficiency of a foliated layer in exchanging heat and moisture as compared to a nonfoliated surface. Allen and Lemon's (1972) findings were cited which showed that for each square meter of overshadowing foliage there will be about 7 m^2 of leaf surface. Deardorff complemented

---

*Deardorff uses an approach similar to Priestley's, except that the coefficients of heat and evaporation (Priestley's K_H and K_W) were treated as functions of the fractional foliage cover and atmospheric stability.

this factor of 7 by an additional 10 percent to account for "stalks, stems, twigs, and limbs which exchange heat but do not transpire."

In the Deardorff approach the 7.7 factor scaled directly with the sensible heat flux. Thus a 1 K temperature difference between the ground/foliage and the air would be about 8.7 (7.7 plus the 1 for the ground) times more effective in transfering heat into the air than would a bare surface with a similar temperature differential. In the new methodology, a flux profile technique is modified to account for a foliated layer. In this approach Thom's (1972) findings were deemed highly applicable.

2.1.7 Adapting Thom's Resistance Model to a Calculation of Sensible Heat

In his paper Thom states "The aerodynamic resistance [r_P] encountered at a rough surface by a property flux will in general exceed the resistance encountered there by the accompanying flux of momentum [r_a]. This excess is conveniently expressed, non-dimensionally by the parameter B^{-1} ... for the property 'P'."

$$B_P^{-1} = u_*(r_P(z) - r_a(z)). \tag{22}$$

In perhaps more plain English, Thom is speaking about a technique called the resistance method. In the resistance method, the property fluxes of heat, momentum, and humidity are treated much like the currents (I) in electrical circuits. Similarly the temperature, humidity, or kinetic energy differences between the air at station height and at the surface can be likened to potential differences (V), while the resistance to the flow (r) is a parameter derived from surface characteristics and the wind structure. The flow rate is thus found from the relation $I = V/r$.

Thom quantizes the baseline atmospheric resistance (resistance to momentum flux) as

$$r_a(z) = \frac{u(z)}{u_*^2}. \tag{23}$$

His equation for r_P (the environmental resistance to the flux of property P) is

$$r_P(z) = \frac{1}{u_*}\left|\frac{\chi_z - \chi_m}{\chi_*}\right|_P. \tag{24}$$

In the case of sensible heat, χ_z is the temperature at height z, θ_z; χ_m is the mean surface temperature, θ_e;* and χ_* is the friction concentration of temperature, T_*. Equation (24), when applied to sensible heat fluxes, is thus rewritten as

$$r_H(z) = \frac{1}{u_*}\left|\frac{\theta_z - \theta_e}{T_*}\right|. \tag{25}$$

---

*θ_e shall also be referred to as the effective surface temperature.

(The use of the term T_*, as opposed to θ_*, is not accidental. It has historical significance. T_* contains a k within its definition (see Kunkel and Walters (1983) or Hoffert and Storch (1979), for example), while θ_* does not (Paulson, 1970).)

The nondimensionalized excess resistance to heat (B_H^{-1} from equation (22)) could now be written from equations (23) and (25). However, a more helpful result is obtained using an additional contribution by Thom. For B_H^{-1} Thom developed the parameterization

$$B_H^{-1} = 6.27\, u_*^{\frac{1}{2}}. \tag{26}$$

Therefore, combining equations (22), (23), and (26), r_H can be solved directly.

$$r_H(z) = \frac{B_H^{-1}}{u_*} + \frac{u(z)}{u_*^2}. \tag{27}$$

From the definition of T_*, the ratio within the absolute value sign in equation (25) will always be positive. The absolute value may therefore be removed, and T_* can be solved for directly from equations (27) and (25).

$$T_* = \frac{(\theta_z - \theta_e)\, u_*}{(B_H^{-1} u_* + u)}. \tag{28}$$

The T_* thus developed is applicable to a fully vegetated layer.

At this point the definition for T_* could be used to calculate the sensible heat in equation (21). However, the interactions for a nonfoliated surface should be considered and merged with result (28) for foliated surfaces so that a final equation will apply for any level of foliation.

In this regard, the results of Kunkel and Walters (1983) were specifically tailored for a nonfoliated surface: Their results included a laminar sublayer parameterization to handle a completely barren surface.

The Kunkel and Walters form for sensible heat flux is written as

$$H_{Sh} = \rho C_P\, u\, c_H\, (\theta_e - \theta_z). \tag{21a}$$

By comparison, the Thom equivalent form for sensible heat flux is written

$$H_{Sh} = \rho C_P \frac{(\theta_e - \theta_z)}{r_H(z)}. \tag{21b}$$

The definition for θ_e used in equation (21a) is

$$\theta_e = \frac{(\theta_g + 1.1\, N \theta_f)}{(1 + 1.1\, N)}, \tag{29}$$

where

$$N = 7\sigma_f. \tag{30}$$

The coefficient value of 7 was derived by Deardorff from findings reported by Allen and Lemon (1972) (for a corn crop) and by Monteith *et al.* (1965) (for a barley crop) that for each square meter of overshadowing foliage, there will be about 7 m^2 of leaf surface area. The factor 1.1 represents an additional 10 percent surface area that accounts for "stalks, stems, twigs, and limbs which exchange heat but do not transpire." The 1.1 factor therefore appears in the sensible heat flux equation, but not in the latent heat flux equations.

The effective temperature of the surface thus represents a weighted average (based on exposed surface area) of the temperatures of the soil (through θ_g) and the foliage (through θ_f). Since the surface area of the leaves can be proportionally much greater than that of the soil, the influence of the ground will be considerably reduced when a heavily foliated layer is present. The use of an effective surface temperature in equation (29) represents the means used to correct the equation for heat flux proposed by Deardorff for the overestimation problem mentioned previously. The weighting function allows the heat flux to be ***proportionally influenced*** by the foliage, but the overall level of the flux will not be vastly greater simply due to the increased surface area presented by the foliage.

Simple comparison of equations (21a) and (21b) shows the only difference between the Kunkel/Walters and Thom equations for sensible heat are the $c_H u$ factor used by Kunkel/Walters and the r_H^{-1} factor used by Thom. Let us now consider in some detail the functional form of these two approaches since the simple appearance of c_H is deceptive. In Kunkel/Walters, the form used for the c_H equation is

$$c_H = \frac{k^2}{0.74\,(\ln \frac{z}{z_0} - \psi_m)(\ln \frac{z}{z_0} - \psi_h + k\,T'/0.74)},$$

where T' was derived from the bluff body form of Garratt and Hicks (1973), ψ_m and ψ_h are the diabatic influence functions described in section 2.4, z is the height above the surface (which in this case will be set to the station height z_s), z_0 is the roughness length, and k is von Kármán's constant (normally set to 0.4 for rough surfaces).*

T' is given by

$$T' = [0.37\,(30\,u_*\,z_0/\nu)^{0.45}\,Pr^{0.8}],$$

where ν is the kinematic viscosity and Pr is the Prandtl number (equal to 0.72 for air). The kinematic viscosity is a function of the dynamic viscosity (μ) and the density of air (ρ), defined as (Smithsonian Meteorological Tables, 1951)

$$\nu = \mu/\rho.$$

---

*Kunkel and Walters use the terms $\ln(z/z_0) + \psi_m$ and $\ln(z/z_0) + \psi_h$, but neither of these usages are common, and in their equations they merely use definitions for ψ_m and ψ_h that are the negative of those commonly used. Therefore, their terminology has been normalized to that of the common usages.

The Smithsonian Meteorological Tables also define μ as

$$\mu = \frac{296.16 + 120}{T + 120} \frac{T^{3/2}}{296.16^{3/2}} = \frac{T^{3/2}}{12.247(T + 120)},$$

where T is the air temperature in Kelvin, and ρ is

$$\rho = 0.34838\, P/T,$$

where P is the pressure in millibars, and the resulting density is in kg/m^3. A simple approximation to the density as a function of height above sea level (a.s.l.) for altitudes less than 15 km a.s.l. has been empirically derived by A. Blanco of BE.

$$\rho = 1.225 - \frac{H}{10}\left[1.176 - \frac{H}{100}\left[4.34 - 7.46\frac{H}{100}\right]\right],$$

where H is the height a.s.l. in kilometers.

The equation for $k\,T'$ therefore reduces to

$$k\,T' = 0.5258\,(u_* z_0/\nu)^{0.45}. \tag{31}$$

Since the air referred to in the equations that require ν is only a few millimeters away from the ground, θ_g may be safely substituted for T in the density and dynamic viscosity equations above.

Let us now compare the terms

$$c_H\, u \rightleftharpoons 1/r_H(z),$$

where the $\rightleftharpoons$ symbol is used to denote a comparison operation, where like quantities in two dissimilar developments are used on either side of the symbol. If the Thom form for r_H and the Kunkel and Walters form for c_H are introduced, we have the relation

$$c_H\, u = u_* \frac{k}{0.74\,(\ln \frac{z}{z_0} - \psi_h) + k\,T'} \rightleftharpoons \frac{u_*}{u/u_* + B_H^{-1}} = \frac{1}{r_H},$$

where the definition (Paulson, 1970)

$$u_* = k\,u/(\ln(z/z_0) - \psi_m)$$

was introduced on the left-hand side. Now, canceling u_*'s on both sides of the equation, dividing by k, inverting both sides, and again utilizing the definition of u_*, one finds

$$0.74\,(\ln \frac{z}{z_0} - \psi_h) + k\,T' \rightleftharpoons (\ln \frac{z}{z_0} - \psi_m) + k\,B_H^{-1}.$$

The use of the 0.74 factor was once believed necessary to compare the parameterized temperature structure to the parameterized wind structure (Businger, 1973), but this was

based on errors committed during the reduction of a set of tower data. Upon reëxamination of the data (Wieringa, 1980), theorists have tended to set the 0.74 constant back to 1.00, as it was according to previous theory. Thus the log terms can be removed and the result is

$$-\psi_h + k\,T' \rightleftharpoons -\psi_m + k\,B_H^{-1}.$$

Once $k\,T'$ and $k\,B_H^{-1}$ are written as functions of u_*, the interrelationship between these approaches becomes even clearer.

$$k\,T' = 0.5258\left(\frac{z_0}{\nu}\right)^{0.45} u_*^{0.45} \rightleftharpoons 6.27\,k\,u_*^{1/3} = k\,B_H^{-1}.$$

Thus an analysis of the two approaches finally leads to comparable terms that scale as fractional powers of the friction velocity in both cases. This analysis reveals that, for what would appear to be dissimilar surfaces (bare ground and foliated layer), similarities still exist in the wind interactions. Perhaps most of the difference in exponents can be attributed to the ability of plants to yield to the wind without being displaced, while soil may be physically transported once its static friction force is overcome, but normally remains in a fixed orientation relative to the wind flow.

Regardless of these differences, the results of the two approaches are similar and a combination of the effects of both responses is desired. To accomplish this combination a mixing coefficient is necessary. A linear mixing based on the fractional foliage cover was at first considered. However, since the roughness length z_0 increases rapidly as the roughness elements increase in size, a linear mixing model would apply a considerably higher surface roughness length to the $k\,T'$ term than would be justified by the conditions under which the equation itself was developed (only designed for smooth surfaces with virtually no foliage). In considering the form for the mixing rule and the rule's relationship to the roughness length (which depends on the surface's drag effects on the wind profile), a new means of approximating z_0 was also considered.

Ideally, the roughness length should depend on the type, height, and fraction of the surface covered by foliage and on the type and size of the grains/pebbles/rocks on the ground beneath the plants. For suitable drag effects, the following rule is proposed as an ad hoc solution, based on the fractional foliage cover and estimates of the roughness lengths due to foliage (z_{0f}) and ground below (z_{0g}).

$$z_0 \approx \sigma_f^{1/3}\,z_{0f} + (1 - \sigma_f^{1/3})\,z_{0g},$$

where $z_{0g} \ll z_{0f}$. For example, a grass covering (roughness elements 2" to 5" high implies $z_{0f} \approx 1$ cm) over a sandy soil (roughness elements 1/16" to 1/2" high implies $z_{0g} \approx 0.06$ cm) with $\sigma_f = 0.5$ would yield an equivalent roughness length of 0.81 cm. In essence

this rule states that the roughness parameter rapidly assumes a value characteristic of the tallest roughness elements as the fraction of those elements over the surface increases.*

Therefore a $\sigma_f^{1/3}$ parameter is used in the mixing rule, rather than σ_f, to allow for a much more rapid transition from a smooth, nonfoliated surface to a foliated surface dominated by interactions with the plants rather than the ground surface.

The resultant equation for $r_H(z)$ uses a linear mixing rule with $\sigma_f^{1/3}$ as the mixing parameter and the two terms $(k\,B_H^{-1} - \psi_m)$ and $(k\,T' - \psi_h)$ as the terms to be mixed. Once mixed, they are replaced in the original Thom equation for resistance, yielding

$$r_H(z) = \frac{\ln\left(\frac{z}{z_0}\right) + \sigma_f^{1/3}(k\,B_H^{-1} - \psi_m) + (1 - \sigma_f^{1/3})(k\,T' - \psi_h)}{k\,u_*}. \tag{32}$$

Using the resistance form for the sensible heat flux above a mixed layer (equation (21b) with equation (32) for r_H), H_{Sh} can be effectively divided into its components due to the surface and the foliage, respectively, by using the definition of θ_e

$$\theta_z - \theta_e = \frac{(\theta_z - \theta_g)}{(1 + 1.1\,N)} + (\theta_z - \theta_f)\left(\frac{1.1\,N}{1 + 1.1\,N}\right).$$

Thus,

$$H_{Sh} = H_{Sg} + H_{Sf}, \tag{33a}$$

$$H_{Sg} = \left[\frac{\rho C_P(\theta_g - \theta_z)}{r_H}\right]\left(\frac{1}{1 + 1.1\,N}\right), \tag{33b}$$

$$H_{Sf} = \left[\frac{\rho C_P(\theta_f - \theta_z)}{r_H}\right]\left(\frac{1.1\,N}{1 + 1.1\,N}\right). \tag{33c}$$

In the program these relations are simplified through the use of the constants

$$A_a = \frac{\rho C_P}{r_H}\left(\frac{1}{1 + 1.1\,N}\right), \tag{34a}$$

$$A_{aa} = 1.1\,N\,A_a, \tag{34b}$$

such that

$$H_{Sg} = A_a(\theta_g - \theta_z), \tag{35a}$$

---

*The accuracy of the 1/3 exponent used may be disputed, but the point is clear: In attempting to meld the two approaches it is necessary to avoid applying the smooth surface result of Kunkel and Walters to a case where the roughness length is much longer than the conditions for which the term $k\,T'$ was developed. Otherwise $0.5258\,(z_0/\nu)^{0.45} \gg 6.27\,k$, and the smooth surface correction term may exceed the foliage correction component, which is physically unrealistic.

$$H_{Sf} = A_{aa}(\theta_f - \theta_z). \tag{35b}$$

In a similar manner, individual latent heat fluxes from ground and foliage are found in the next section. Notice, however, that the sensible heat fluxes from soil and foliage are assumed to be completely independent. In the real world the plants could possibly heat up first and thereby warm the ground. This effect is not modeled. The assumption is that any interactions between ground and foliage will be through radiant fluxes rather than through sensible or latent heat fluxes.

2.1.8 Latent Heat Flux for a Foliated Layer

In the Deardorff approach to moisture transfer, only that fraction of the surface that is considered to be *moist* may be involved in evapotranspiration. The parameters controlling these fractions are r'' and α' for the fractional moist foliage and ground surfaces, respectively. The weighted mean fraction of the surface susceptible to evaporation can thus be modeled through the parameter

$$A' = \frac{\alpha' + r''N}{(1+N)}. \tag{36}$$

The terms α' and r'' are based on Deardorff (1978) and given as

$$\alpha' = (1 - \delta_c) + \min(1,\, w_g/w_k)\,\delta_c,$$

$$r'' = 1 - \delta_c\,[r_s/(r_s + r_a)]\,[1 - (w_{dew}/w_{dmax})^{2/3}],$$

$$\delta_c = \begin{cases} 1, & \text{evaporation is occurring,} \\ 0, & \text{condensation is occurring,} \end{cases}$$

where w_g is the fractional moisture of the ground (by volume); w_k is the fraction of moisture the ground contains when it behaves as if it is saturated; r_s is the stomatal resistance; r_a is the atmospheric resistance; w_{dew} is the mass per unit ground area of dew on the foliage (normally zero during the day); and w_{dmax} is the maximum dew accumulation before runoff to the ground will occur. Further equations for r_s, r_a, and w_{dmax} can be found in Deardorff (1978). These equations depend on the foliage type, wilt factors, mean incident sunlight, and other coupling factors, which will not be explained here. The controlling parameters are generated in the model, and no justification for the validity of Deardorff's approach will be presented. Note that evaporation is considered to be occurring if $Q_{sat}(\theta_g) > Q_z$ or $Q_{sat}(\theta_f) > Q_z$, depending on whether the ground or foliage surfaces are being considered.

Using a flux equation form similar to that in Paulson (1970), the total latent heat flux can be described by the equation

$$L_v E_h = -\rho\, L_v\, Q_*\, u_*. \tag{37}$$

Or, using the same method used to develop the heat equation,

$$L_v E_h = \rho\, L_v \frac{(Q_e - Q_z)}{r_Q}, \tag{38}$$

where $r_Q = r_H$, since all fluxes other than momentum flux are due to conservative passive additive transport processes and the same dynamics should regulate each. Note in these flux equations that the A' term used by Deardorff is handled implicitly in the $Q_e - Q_z$ difference term.

Having defined A' (equation (36)), and since L_v is the latent heat of vaporization (equal to 2.5008×10^6 J/kg) and Q_z is the specific humidity of the air at height z ($Q_z = R_H\, Q_{sat}(T_z)$ [see appendix A for computation of $Q_{sat}(T)$]), all that remains is to determine Q_e. The Q_e used in equation (38) must be related to the Q_{sat} values of the leaf and ground surfaces. Using a combination of equations derived by Deardorff and the same weighted averaging technique used in the sensible heat flux derivation, one can model the appropriate surface effective specific humidity as

$$Q_e = \frac{\alpha' Q_{sat}(\theta_g) + r'' N\, Q_{sat}(\theta_f)}{(1+N)}. \tag{39}$$

This weighting method emphasizes that the equivalent specific humidity of the surface is related to both the relative availability of water on the ground and leaf surfaces and the proportional area of the surface occupied by the given surface type. Also, the 1.1 term is not used because the stems, twigs, and so forth do not transpire. The weighting achieved is similar to weighting the $Q_{sat}(\theta_z)$ by the relative humidity.

With these definitions for the quantities governing the overall flux of moisture, the total latent heat flux may be broken into its respective ground and foliage related components

$$L_v E_h = L_v E_g + L_v E_f, \tag{40a}$$

where the constituent fluxes are

$$L_v E_g = \frac{\rho L_v (Q_{sat}(\theta_g) - Q_z/A')}{r_Q} \left(\frac{\alpha'}{1+N}\right), \tag{40b}$$

$$L_v E_f = \frac{\rho L_v (Q_{sat}(\theta_f) - Q_z/A')}{r_Q} \left(\frac{r'' N}{1+N}\right). \tag{40c}$$

These relationships can be simplified through the use of the constants B_b and B_{bb}

$$B_b = \frac{\rho L_v}{r_Q} \left(\frac{\alpha'}{1+N}\right), \tag{41a}$$

$$B_{bb} = \frac{\rho L_v}{r_Q} \left(\frac{r'' N}{1+N}\right), \tag{41b}$$

so that

$$L_v E_g = B_b (Q_{sat}(\theta_g) - Q_z/A'), \tag{42a}$$

$$L_v E_f = B_{bb} (Q_{sat}(\theta_f) - Q_z/A'). \tag{42b}$$

2.2 Temperature Calculations

The methods of evaluating the various radiative and convective heat fluxes were discussed in the previous section. In this section the means of estimating the foliage and soil temperatures are described.

The Newton-Raphson method is used to search for the foliage temperature solution to equation (2), which can be rewritten as

$$A_{a1}\, S_{h_\downarrow} + A_{a2}\, R_{Lh_\downarrow} + A_{a3}\, \theta_g^4 - A_{a4}\, \theta_f^4 = H_{Sf} + L_v E_f, \tag{43}$$

where

$$A_{a1} = (1 - \alpha_c) - (1 - \alpha_g)(1 - \sigma_f)\, A_{\infty(l)}, \tag{44a}$$

$$A_{a2} = 1 + \sigma_f\,(1 - \epsilon_g)(1 - \sigma_f)\, A_{\infty(l)} - \sigma_f\,(1 - \epsilon_f) - (1 - \sigma_f)\, A_{\infty(l)}, \tag{44b}$$

$$A_{a3} = \sigma\, \epsilon_g\, \sigma_f\, \epsilon_f\, A_{\infty(l)}, \tag{44c}$$

$$A_{a4} = \sigma\, \epsilon_f\, \sigma_f\, [1 + A_{\infty(l)} - \sigma_f\,(1 - \epsilon_g)\, A_{\infty(l)}]. \tag{44d}$$

To elucidate further on the components of the A_{ai} constants: A_{a1} has two terms. The first term represents the incident direct solar (the 1) and the reflected direct solar ($-\alpha_e$). The second term represents the energy that passes through the layer, $-(1 - \sigma_f)$, and the energy that returns after reflection from the soil, $\alpha_g\,(1 - \sigma_f)$.

A_{a2} has four terms. The first term represents the incident longwave radiation from the sky. The second term represents the energy travelling upward toward the foliage layer following an initial passage through the layer and a reflection at the surface. The third term represents the energy that travels upward from the top of the foliage. The fourth term represents the energy that travels downward from the bottom of the foliage layer toward the surface.

A_{a3} has only the single term related to absorption by the foliage layer of energy emitted by the soil.

A_{a4} has three terms. The first term relates to the upward thermal emissions from the foliage. The second and third terms refer to the energies that flow between the foliage layer and the soil that originated as graybody radiation at the foliage layer.

If the constant terms are gathered together, a single function of θ_f may be formed. Let

$$A_{b1} = A_{a1}\, S_{h_\downarrow} + A_{a2}\, R_{Lh_\downarrow} + A_{a3}\, \theta_g^4 + A_{aa}\, \theta_z + B_{bb}\, Q_z / A'. \tag{44e}$$

Equation (43) can then be written as

$$F(\theta_f) = -A_{b1} + A_{a4}\, \theta_f^4 + A_{aa}\, \theta_f + B_{bb}\, Q_{sat}(\theta_f) = 0. \tag{45}$$

To solve for $F(\theta_f) = 0$ using Newton-Raphson, the previous value of foliage temperature is used as the initial value in the iterative equation

$$\theta_{f_{(n+1)}} = \theta_{f_{(n)}} - \frac{F}{F'} \tag{46}$$

until the equation converges, where the term F' is given by

$$F' = 4\,A_{a4}\,\theta_f^3 + A_{aa} + B_{bb}\frac{dQ_{sat}(\theta_f)}{d\theta_f}. \tag{47}$$

The definition of Q_{sat} and its derivative are discussed in appendix A.

In this derivation the assumption is that θ_g is known while making the computations to estimate θ_f. But, we cannot know θ_g unless we know θ_f, which leads to a circular argument. This dilemma is "solved" in this model by using the θ_g from the previous time step. Such an assumption avoids certain problems due to mathematical instabilities in the model that might otherwise arise. It should be a good assumption, as long as the time increment used in updating the soil temperature is reasonably short, since the soil temperature (which includes an inertia term) will vary more slowly than the foliage temperature. The foliage temperature calculation then has a unique solution.*

Once the foliage temperature has been estimated, the new ground temperature is found using the Crank-Nicholson method. This method assumes the time step (Δt) is small enough that fluxes at time $t_{(n+1)}$ can be determined based on the temperature value at time $t_{(n)}$ ($\theta_{g_{(n)}}$) and the temperature difference ($\theta_{g_{(n+1)}} - \theta_{g_{(n)}}$) across the time step. For example, the flux of thermal radiative emissions from the ground is proportional to the temperature to the fourth power. This is approximated at the new time by

$$\theta^4_{g_{(n+1)}} \approx \theta^4_{g_{(n)}} + 4\,\theta^3_{g_{(n)}}\,(\theta_{g_{(n+1)}} - \theta_{g_{(n)}}). \tag{48}$$

Similarly, the new saturated specific humidity is approximated based on its present value and a change with temperature of

$$Q_{sat}(\theta_{g_{(n+1)}}) \approx Q_{sat}(\theta_{g_{(n)}}) + \left(\frac{\partial Q_{sat}}{\partial \theta}\right)_{\theta_{g(n)}} (\theta_{g_{(n+1)}} - \theta_{g_{(n)}}). \tag{49}$$

The fluxes during the period covered by the time step are treated using average values for the fluxes. The averaged temperature dependencies for sensible, longwave, and evaporative heat fluxes are

$$\theta_g \approx \frac{(\theta_{g_{(n+1)}} + \theta_{g_{(n)}})}{2}, \tag{50a}$$

$$\theta^4_g \approx 2\,\theta^3_{g_{(n)}}\,\theta_{g_{(n+1)}} - \theta^4_{g_{(n)}}, \tag{50b}$$

$$Q_{sat}(\theta_g) \approx Q_{sat}(\theta_{g_{(n)}}) + \frac{(\theta_{g_{(n+1)}} - \theta_{g_{(n)}})}{2}\left(\frac{\partial Q_{sat}}{\partial \theta}\right)_{\theta_{g(n)}}. \tag{50c}$$

---

*However, when reëvaluating F and F' at each step in the Newton-Raphson approach, it is necessary to consider changes in r'', since when on the borderline between evaporation and condensation, r'' can vary widely depending on the value of θ_f.

All the heat fluxes in equation (3) can now be written as functions of $\theta_{g_{(n)}}$ and $\theta_{g_{(n+1)}}$. These quantities may then be substituted for G in equation (4), and the remaining terms in equation (4) can also be expressed as functions of $\theta_{g_{(n)}}$ and $\theta_{g_{(n+1)}}$. The resulting equation can then be separated into that portion that depends on $\theta_{g_{(n+1)}}$ and on the remaining terms that are considered constant. Since the resulting function is linear in $\theta_{g_{(n+1)}}$, $\theta_{g_{(n+1)}}$ is found to equal the ratio of two sets of terms. Following this approach, one can rewrite equation (4) as

$$\frac{(\theta_{g_{(n+1)}} - \theta_{g_{(n)}})}{\Delta t} = \frac{c_1 G}{I_1} + \frac{c_2 \theta_2}{\tau_{day}} - \frac{c_2 (\theta_{g_{(n+1)}} + \theta_{g_{(n)}})}{2 \tau_{day}}, \tag{51a}$$

$$\theta_{g_{(n+1)}} \left[\frac{1}{\Delta t} + \frac{c_2}{2 \tau_{day}} \right] = \frac{c_1 G}{I_1} + \frac{c_2 (2\theta_2 - \theta_{g_{(n)}})}{2\tau_{day}} + \frac{\theta_{g_{(n)}}}{\Delta t}, \tag{51b}$$

where the G term must still be divided between constants and terms linear in $\theta_{g_{(n+1)}}$. This task is accomplished in the equation

$$G = S_{net} + R_{Lg2} - C_{\theta_{g_{(n)}}} + \Gamma_1 \theta_{g_{(n+1)}}, \tag{52}$$

where

$$S_{net} = (1 - \alpha_g)(1 - \sigma_f) S_{h_\downarrow} A_{\infty(s)}, \tag{53a}$$

$$R_{Lg2} = \epsilon_g A_{\infty(\ell)} \{(1 - \sigma_f) R_{Lh_\downarrow} + \sigma_f \epsilon_f \sigma \theta_f^4 - [\sigma_f (1 - \epsilon_f) - 1] \sigma \theta_{g_{(n)}}^4\}, \tag{53b}$$

$$C_{\theta_{g_{(n)}}} = A_a (\theta_{g_{(n)}}/2 - \theta_z) + B_b \left(Q_{sat}(\theta_{g_{(n)}}) - \frac{\theta_{g_{(n)}}}{2} \left(\frac{\partial Q_{sat}}{\partial \theta} \right)_{\theta_{g_{(n)}}} - \frac{Q_z}{A'} \right), \tag{53c}$$

$$\Gamma_1 = 2 \epsilon_g \sigma \theta_{g_{(n)}}^3 A_{\infty(\ell)} [\sigma_f (1 - \epsilon_f) - 1] - \frac{A_a}{2} - \frac{B_b}{2} \left(\frac{\partial Q_{sat}}{\partial \theta} \right)_{\theta_{g_{(n)}}}. \tag{53d}$$

Thus the solution for the ground temperature value at the next time step is

$$\theta_{g_{(n+1)}} = \frac{\left[\frac{c_1 (S_{net} + R_{Lg2} - C_{\theta_{g_{(n)}}})}{I_1} + \frac{c_2 (2\theta_2 - \theta_{g_{(n)}})}{2 \tau_{day}} + \frac{\theta_{g_{(n)}}}{\Delta t} \right]}{\left[\frac{1}{\Delta t} + \frac{c_2}{2 \tau_{day}} - \frac{c_1 \Gamma_1}{I_1} \right]}. \tag{54}$$

2.3 Modeling Additional Air, Soil, and Plant Parameters

In this section the equations related to θ_2, conservation of moisture, and θ_z are discussed. Also, parameters that evolve with time due to their dependence on moisture are considered.

2.3.1 Moisture and Temperature Equations

In addition to the surface and foliage temperatures, the deep ground temperature θ_2 and the flux dependent near surface air temperature θ_z must be computed. The first of these equations is quite simple, being derived from equation (6), using the stepping methodology devised for the ground temperature that was discussed in the previous section:

$$\frac{\theta_{2_{(n+1)}} - \theta_{2_{(n)}}}{\Delta t} = \frac{G}{I_2},$$

whence

$$\theta_{2_{n+1}} = \theta_{2_n} + \frac{\Delta t\, G}{I_2}.$$

The net flux into the ground, G, is known as a by-product of computing the new temperature $\theta_{g_{(n+1)}}$ (equation (52)).

A similar equation to that developed for θ_g is used to determine the updated values for the soil moisture parameters w_g and w_2. The change in w_g is modeled as

$$\frac{w_{g_{(n+1)}} - w_{g_{(n)}}}{\Delta t} = -C_1 \frac{(E_g + 0.1\,E_f - P_{recip})}{\rho_w\, d_1'} - C_2 \frac{(w_g - w_2)}{\tau_{day}}, \qquad 0 \le w_g \le w_{max}, \quad (55)$$

where P_{recip} is the amount of precipitation measured in kg/(m^2 s), d_1' is the distance 10 cm, w_{max} is the maximum fraction of moisture the near surface ground can contain before runoff occurs, ρ_w is the density of water (1000 kg/m^3), and the constants C_1 and C_2 are weighting terms based on the work of Jackson (1973) (see Deardorff, 1978). As seen from the above equation, the modeled surface moisture depends on transpiration, evaporation, and precipitation in the first term on the right and on a restoring flow of moisture up through the ground from the deeper layer.

Similar to the computation for θ_2, the computation of w_2 depends on the overall flux of moisture through the surface.

$$\frac{w_{2_{(n+1)}} - w_{2_{(n)}}}{\Delta t} = -\frac{(E_g + E_f - P_{recip})}{\rho_w\, d_2'}, \quad (56)$$

where d_2' is the distance 50 cm. Notice that the w_g equation only incorporates 1/10th of the E_f transpiration flux. This is because the Deardorff model assumes the roots of the plants extend deeper than the surface layer. Note also that the constants C_1 and C_2 depend on empirical rules simulating the capillarity and other transport properties of the soil. Deardorff provides no information other than single constants for these terms, which have no direct relation to physically measureable quantities.

The estimation of the near surface air temperature, θ_z, is somewhat more problematic since the temperature will depend not only on the measured air temperature and the estimated sensible heat flux but also on the characteristic depth of mixing expected under

the present condition of the atmospheric stability.* Based on these assumptions, the mixing rule developed is

$$\theta_{z_{(n+1)}} = \theta_{z_{(n)}} \left(1 - \frac{\Delta t}{720}\right) + \theta_a \frac{\Delta t}{720} + \frac{H_{Sh}\,\Delta t}{\rho C_P Z_{inv}}, \tag{57}$$

where,

$$Z_{inv} = 50\,u \tag{58}$$

is an ad hoc estimate of the mixing depth of the atmosphere. The constant 720 reflects the idea that the maximum lag time allowed in the model between measured temperature θ_a and modeled temperature θ_z is only half a day of model time and allows for seasonal and synoptic influences on the energy budget. The term varying with sensible heat means the near surface air temperature will respond to the diurnal cycles of warming and cooling that occur.

2.3.2 Moisture Dependent Coefficients

Perhaps after computing the fluxes and temperatures, one might imagine they could completely characterize the turbulent structures and vertical mean profiles. This is possible, if the total simulated time is short. However, first, the model requires at least a few hours of simulated running time to settle down from its initialization (due to the thermal inertia term). Second, if the model is run so as to simulate a few days time, the soil moisture parameters will alter the soil thermal characteristics. This bookkeeping can be handled between the temperature computations at each time step.

Deardorff gave parameterized equations to allow the heat conduction, heat capacity, and surface reflectivity to vary with the soil moisture. In suggesting a modification on the Deardorff approach, one might allow a user to designate a set of standard soil types or input unique initial conditions. As the model runs, these variables are modified by the change in water content from the initial conditions as follows:

$$\rho_s c_s = (\rho_s c_s)_0 + 4.184 \times 10^6\,(w - w_0), \tag{59a}$$

$$\rho_s c_s \kappa_s = \lambda = \lambda_0 + \kappa_s \times 4.184 \times 10^6 \left(\frac{w^{1/3} - w_0^{1/3}}{w_{max}^{1/3}}\right), \tag{59b}$$

$$\alpha_g = \alpha_0 - 0.17\,\frac{(w_g - w_{g_0})}{w_k}, \tag{59c}$$

where $\rho_s c_s$ is the soil heat capacity (soil density times the specific heat capacity), $\rho_s c_s \kappa_s$ is the thermal conductivity (with κ_s the thermal diffusivity), and α_g has already been

*Note that latent heat is not expected to contribute to the temperature change in the atmosphere, and in local thermodynamic equilibrium there should be no significant radiative contributions either.

given as the soil mean reflectivity in the shortwave band (albedo). The first two equations have been applied to the surface (w_g) and deep soil (w_2) thermal parameters. These equations parallel Deardorff's equations (37), (38a), and (40). Different standard soil types, with associated nominal properties, were included in the TGRAD model as options. The soil properties were derived from average soil conditions as documented by Oke (1978), Deardorff (1978), and Link (1979). The final equation is applied at the surface, and TGRAD utilizes reflectivity coefficients derived from the same sources.

2.3.3 Possible Improvements

In addition to variation under changing moisture in the soil, it is possible to configure a program to treat snow cover and freezing conditions. Such a model would be beneficial in approximating a European climate. However, the scope of such a model is very broad, covering the various aspects of adding a new layer in the temperature flux computations for the snow, of adding the additional considerations of conversion of water to ice and ice to water, and of adding various other complexities. As such, a model overing these topics would be a subject unto itself. The model described here is not designed to make a transition through freezing or thawing conditions.

Note also that the temperature of precipitation may influence the soil temperature calculation, but was excluded. From a practical standpoint, the structure of the atmosphere will normally be neutral during any precipitation episode.

Another consideration is in regard to the seasonal variation of the stomatal resistance of plants to evapotranspiration. For the stomatal resistance equation, Deardorff indicates that "in temperate latitudes, $\mathcal{S}$ (the stomatal resistance's seasonal dependence factor) is set to zero during the growing season and to a value much larger than unity during the rest of the year." In the program, $\mathcal{S}$ is set to 50 except during a European growing season. For desert conditions $\mathcal{S}$ is assumed to remain high year-round, since, for most plants, survival requires high transpiration resistance. Relatively little is known about the stomatal resistance of the various weeds and scrub brush normally encountered in actual tactical terrains and during field measurements, since most studies have focused on crop characteristics. A comprehensive study of the properties of general vegetation would be in order, to truly obtain a more rigorous model.

The present model is designed to include sequential inputs of data and compute the resulting atmospheric states as a time series. However, the model could be reconfigured relatively simply so that it could run a single day case, reinitializing the soil parameters at an appropriate time each day. This step is possible using simple bookkeeping techniques, whose details need not be considered further here. The advantage of such a modification would be to allow for the settling down of any transient behavior to obtain a repetitive (cyclical) response of the model to a single day's input data set.

2.4 Bulk Aerodynamic Parameters

In the derivation of the equation for sensible heat, the terms u_*, ψ_m, and ψ_h were introduced, but not defined mathematically. The definitions are provided in this section, finally completing the description of the means of estimating the surface heat fluxes. In addition, the purpose of the model was not merely to compute the ground and foliage temperatures. Rather, the computations were a step toward characterizing the vertical structures of temperature, refractive index, refractive index structure parameter, inner and outer scales, and windspeed. Therefore, in this section, the flux profile forms for the vertical structures are introduced and the means of estimating u_*, ψ_m, and ψ_h are given, along with the vertical structure equations for the other parameters.

One of the principle scaling parameters used in flux profile theory is the Obukhov length. To estimate the friction velocity u_* and aerodynamic resistance r_H, the Obukhov length must also be computed. This length is defined as

$$L = -\frac{\rho C_P \theta_z u_*^3}{k g H_{Sh}}, \tag{60}$$

where g is the gravitational acceleration. The friction velocity is found as a function of the Obukhov length.

$$u_* = \frac{k u}{(\ell n \left(\frac{z}{z_0}\right) - \psi_m)}, \tag{61}$$

where z_0 is the roughness height, z is the height above the surface where u is to be measured, and ψ_m is the diabatic influence function for momentum. Of course, once u_* has been estimated, the vertical structure of windspeed can be determined simply by inverting equation (61) to compute

$$u = \frac{u_*}{k}(\ell n \left(\frac{z}{z_0}\right) - \psi_m). \tag{62}$$

The correct definition of z must be handled carefully since it is defined with respect to the vertical structure of the wind profile and not simply with respect to the height above the surface. Foliated layers introduce a correction to the value of z compared to the actual height above a physical surface. In particular, let z_s' be the actual height of the windspeed measuring station above the ground. z_s is related to z_s' through the relation

$$z_s = z_s' - D, \tag{63}$$

where D is called the displacement height. This quantity is found using

$$D = 0.70\,(z_0/0.13). \tag{64}$$

This equation is derived as follows: D is modeled as being approximately 7/10ths of the height of the vegetation. The height of the vegetation is approximately $z_0/0.13$.* Since we previously redefined the roughness length for partially vegetated layers, the D parameter should vary smoothly toward a smaller value as the fractional foliage cover is reduced. Figure 2 shows a representative vertical wind structure pattern when the displacement height is incorporated (after Oke (1978)).

In some models the height of the extrapolated surface value for temperature is also computed. In the approach used in this model, this height difference is accounted for differently through the difference in resistances between momentum and sensible heat fluxes.

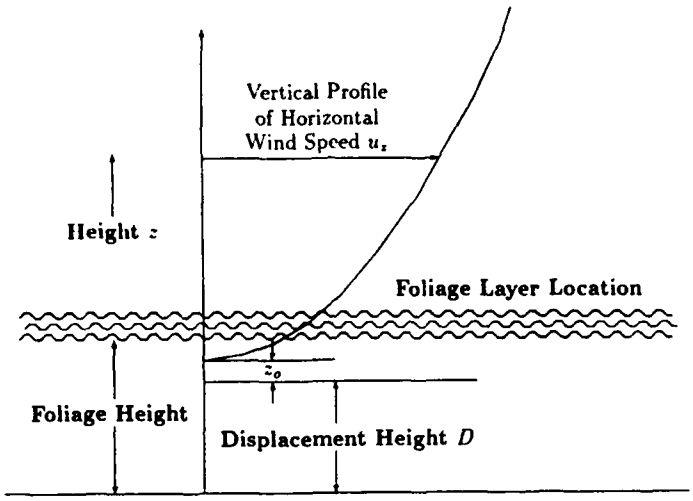

Figure 2. Foliage height H and extrapolated zero of the windspeed profile for a fully foliated layer.

Returning now to the main line of argument, in equation (61) the term ψ_m is the diabatic influence function. (The m stands for momentum and is usually applied as a modifier to the wind profile.) The symbol ψ_h similarly represents the diabatic influence function for sensible heat (h). As ψ_m helps scale the vertical wind profile, ψ_h helps scale the vertical temperature profile.

ψ_m and ψ_h are both functions of height (z) and Obukhov length and have different mathematical forms depending on the stability conditions. When the Obukhov length is less than zero (an unstable atmosphere) the ψ functions have the form

$$\psi_m = 2\,\ell n\left(\frac{1+\phi_m}{2\phi_m}\right) + \ell n\left(\frac{1+\phi_m^2}{2\phi_m^2}\right) - 2\tan^{-1}\left(\frac{1}{\phi_m}\right) + \frac{\pi}{2}, \qquad (65a)$$

*Frank Hansen, c. 1990, BE, WSMR, NM, informal communication, indicates the roughness length is usually about 13 percent of the height of the roughness elements. Thus by dividing z_0 by 0.13, the height of the roughness elements is obtained.

$$\phi_m = \left(1 - 15\frac{z}{L}\right)^{-\frac{1}{4}}, \tag{65b}$$

$$\psi_h = 2\,\ell n\left(\frac{1+\phi_h^2}{2\phi_h^2}\right), \tag{65c}$$

$$\phi_h = \left(1 - 15\frac{z}{L}\right)^{-\frac{1}{2}}. \tag{65d}$$

When the Obukhov length is greater than zero (a stable atmosphere) the functions take the form

$$\psi_m = \psi_h = 1 - \phi, \tag{66a}$$

$$\phi_m = \phi_h = \phi = 1 + \beta\frac{z}{L}. \tag{66b}$$

The terms stable and unstable refer to the behavior of a parcel of air at the same temperature with height as its surroundings when that parcel is displaced slightly in a vertical direction. In a stable atmosphere the parcel will attempt to return to the level from which it was displaced (perhaps initiating an oscillatory motion). In an unstable atmosphere the parcel will become warmer or cooler than its environment, depending on whether the displacement was upward or downward, respectively. In this case the force on the parcel will be such that the parcel will move vertically *away* from its level of origin.

Since the Obukhov length is negative for unstable atmospheres and positive for stable atmospheres, it is a useful measure of the current state of the vertical structure of the atmosphere. It approaches either positive or negative infinity under neutral (adiabatic) stability conditions. Normally, the Obukhov length appears in equations in the denominator of a dimensionless length variable such as $\xi = z/L$. Thus there is a smooth transition of the ξ variable across the neutral stability condition between stable (positive) and unstable (negative) atmospheres as L varies.

Although there are several other forms for equations (65) and (66) available in the literature (Yaglom, 1977), the forms chosen were those suggested by Hansen in private communication* and correspond to the equations recommended by Dyer (1974) and Hanna *et al.* (1982).

Notice that we now have a problem: L depends on u_* and H_{Sh}; u_* depends on L; and H_{Sh} depends on u_*, r_H, θ_f, and θ_g. r_h depends (ultimately) on L and u_*; and θ_f and θ_g depend on the H_{Sh}. One can only compute all these variables simultaneously, by using an iterative procedure. This procedure fixes the temperature difference $\theta_e - \theta_z$ and the wind speed u to constant values while L, r_H, H_{Sh}, and u_* are successively calculated until the Obukhov length converges. The foliage and surface temperatures can then be computed. An approximation is therefore made that the constants A_a, A_{aa}, B_b, and B_{bb} will depend on the previous time interval's θ_g and θ_f estimates. As long as the time interval is short,

---

*The β coefficient is equal to the inverse of the critical Richardson number.

this approximation should not lead to significant error. Certainly it is less in error than the approximation of constant flux controlling coefficients.

To simultaneously calculate the above parameters, first u_* is estimated using an assumption of an adiabatic atmosphere. Then, L can be estimated. Subsequently, r_H can be estimated. As discussed in the previous paragraph, θ_g and θ_f will be used in determining the temperature difference between the station height and the surface. Hence, the estimate of the sensible heat flux can be determined immediately after estimating r_H. Once these four steps are complete, the cycle can be repeated to determine an estimate of u_* with the previous (nonadiabatic) value for L and more accurate values of the other parameters. The cycle is halted once the parameters sufficiently approach limiting values.

In following this procedure, unstable atmospheric conditions do not present a problem, and computations always converge. However, for stable atmospheres the equations may become inconsistent. For the moment, ignoring the $k\,B_H^{-1}$ and $k\,T'$ influences on r_H, and since

$$-\psi_m = -\psi_h = \phi - 1 = \beta\, z/L,$$

r_H can be approximated by u/u_*^2. The equation for L thus reduces to

$$L = \frac{\theta_z\, u^2}{g\,(\theta_z - \theta_e)(\ell n(\zeta) + \beta\, z/L)},$$

where $\zeta = z/z_0$. Let us now rewrite this equation,

$$1 = \frac{g\,L\,\ell n(\zeta)\,(\theta_z - \theta_e)}{\theta_z\, u^2} + \frac{\beta\, g\, z\,(\theta_z - \theta_e)}{\theta_z\, u^2}.$$

Notice that under stable atmospheric conditions, L must always be greater than zero. Similarly, θ_z will be warmer than the surface temperature, and β, g, and z are all positive values. Therefore, there are no negative terms on the right side of the equation, and if

$$\frac{\beta\, g\, z\,(\theta_z - \theta_e)}{\theta_z\, u^2} \geq 1,$$

the equation has no solution. Thus for a real solution the condition

$$\beta^{-1} > \frac{g\, z(\theta_z - \theta_e)}{\theta_z\, u^2} \tag{67}$$

must be met. When this condition fails, u_* is set to a minimum value of 0.07 to force a reasonable value for L to be obtained. With u_* fixed, r_H and L are determined directly. This technique is, however, less than optimal, and one would hope for a better understanding of the behavior of the nocturnal surface layer atmosphere. Appendix B includes a small description of the problems encountered at night and some analysis of gravity wave influence on the overall time-based structure of the nocturnal temperature gradient.

The CN subroutine also computes the quantities related to the characterization of the surface layer atmosphere. These include C_n^2, C_T^2, C_V^2, and dT/dz. Kunkel and Walters (1983) provide equations for the C_n^2 and C_T^2 parameters.

$$C_n^2 = (C_T^2(z)\, A^2\, P^2/T_z^4)(1 + 0.03/B)^2, \tag{68}$$

where A is a proportionality constant whose value depends on wavelength. In the visible/infrared region of the spectrum, the value $A = 79 \times 10^{-6}\mathrm{K\ mbar^{-1}}$ is applicable. The quantity B is called the Bowen ratio and is equal to H_{Sh}/LE_h. $C_T^2(z)$ was obtained from Wyngaard (1973) as

$$C_T^2 = T_*^2\, z^{-2/3}\, 4.9(1 - 7\xi)^{-2/3} \tag{69}$$

for unstable conditions, and

$$C_T^2 = T_*^2\, z^{-2/3}\, 4.9(1 + 2.4\xi^{2/3}) \tag{70}$$

for stable conditions.

For C_V^2, Ochs and Hill (1985) recommend the equation

$$C_V^2 = 2\epsilon^{2/3}, \tag{71}$$

where the C_V^2 computed is the longitudinal component (the most significant component for acoustic propagation problems), and ϵ is the energy dissipation rate. Businger (1973) provides an equation for the inner scale as a function of u_* and z under neutral stability conditions.

$$\epsilon = \frac{u_*^3}{k\, z}. \tag{72}$$

Analysis of data measured by Ochs tends to indicate the dependence of ϵ on stability conditions is weak (Tofsted and Auvermann, 1991).* This finding would appear to be in accord with the relationship of C_V^2 with ϵ (C_V^2 is most dependent on the turbulent loss of fluctuation energy due to viscous dissipation. But viscous dissipation is a process related to kinetic collisions of molecules and has little dependence on stability at this small size scale).

---

*The data mentioned was unpublished and was obtained from Gerald Ochs of the Wave Propagation Laboratory (WPL), National Oceanographic and Atmospheric Administration (NOAA), Boulder, CO, c. 1990. The data was a windspeed versus inner scale scatter plot, which has been incorporated into Tofsted and Auvermann (1991). The statement that the data infers minimal dependence of the dissipation rate on stability follows from the derivation of inner scale, which depends on dissipation. Had there been a marked dependence of dissipation on stability, the plot would have had significantly greater scatter than was present, particularly at low windspeeds.

For acoustic and visible refraction, the temperature gradient is given by

$$\frac{dT}{dz} = \frac{d\theta_z}{dz} + \Gamma = \frac{T_*}{k\,z}\,\phi_h(\xi), \tag{73}$$

where Γ is -0.0098 K/m for relative humidities less than about 98 percent and -0.0065 K/m for higher relative humidities.

The equation for the turbulent outer scale was derived from a combination of the parameterization for du/dz, obtained from Paulson (1970), and an equation for outer scale that depends on du/dz obtained from Lewellen (1977).

$$L_o = 1.68\,k\,z\,(1 - 16\,\zeta)^{1/4}, \tag{74}$$

where k is again von Kármán's constant and $\zeta = z/L$.

Finally, an expression for inner scale was derived in Tofsted and Auvermann (1991). This development took an analytical expression for inner scale (Wyngaard, 1973) and modified it by an empirical expression based on data measured at Table Mountain, Colorado, by Ochs. The expression was

$$\ell_o \approx 0.000463 \left[\frac{T_2^{5/2}\, z^{1/3}\, \ell n(z/z_0)}{P\,(T + C)}\right]^{3/4} \left[1 - 0.0618\,u + \frac{0.5148}{u} + \frac{0.2683}{u^2}\right], \tag{75}$$

where $C = 120$ K, T_2 is a 2-m a.s.l. temperature measurement (in degrees Kelvin), and u_2 is a 2-m a.s.l. windspeed measurement (in m/s).

3. SUBROUTINE DESCRIPTIONS

The TGRAD program is designed as a set of interactive subroutines that are based around a main subroutine called TGRAD. The particular form for the main routine is of little consequence to the overall operations of the subroutines and will not be considered in depth here. The reasoning is that any suitable routine that passes the correct information to the subroutines may be used. K. Kunkel (as part of the work leading to Kunkel (1985)) has produced a relatively simple driver routine that is listed in section 4.

3.1 TGRAD

TGRAD is the main subroutine of the code. It is the only routine the main code needs to call. The name TGRAD refers to the routine's estimation of temperature gradient that was the principal purpose of the original code. Since the majority of the code is based on Deardorff (1978), equations based on Deardorff are annotated by the capital D specifier in the source code listing.

The input to TGRAD usually involves data entered through two separate files. In the first, a description of the site is given. This description should not vary significantly

with time. It includes data on the site's latitude, the soil type (such as loam, sand, and clay), the fractional foliage cover, the predominant cloud type, the height at which the atmospheric characteristics (for example, temperature gradient and C_n^2) should be estimated, the surface roughness length, and the degrees of longitude the site is west of the standard meridian. The second file contains the meteorological data from a measurement station (assumed to be 2 m a.s.l.) coupled with the corresponding time information (Julian date and local time for each weather record). The required input data are the windspeed in m/s, temperature in degrees Celsius, fractional cloudcover, pressure in millibars, and relative humidity in percent. This information is passed to TGRAD routine by the driver.

When the routine is called for the first time, a flag will be set to zero, indicating that the routine must set up default initializations of the surface energy budget parameters. If it is not the first time the routine is called, the routine will compute the energy budget based on the new inputs and the variable values stored in the SAVED common block of passed data. (See the list of parameters and/or the program comments for the descriptions of the variables in the various common blocks.) Normally the initialization flag will be set to one, indicating the new data is consistent with what has been provided previously. If gaps occur in the data, a zero can again be passed to the TGRAD routine to allow a new initialization.*

Once the subroutine TGRAD has set up initial conditions (if necessary), soil parameters are also set. Then, the times of sunrise and sunset are found from subroutine SUN, the vapor pressure and specific humidity of the air are found from subroutine SPEHU, groups of constants are found that are used later in the program, and the amount of incident solar radiation is found from subroutine CLOUD. The specifics of these subroutines are discussed in subsequent sections.

Table 1 provides a listing of the variables used in the subroutine and a brief description of each. Table 2 provides a listing of the inputs required to the subroutine and their description.

---

*Such gaps have occurred when the model was used to predict the behavior of the surface layer atmosphere from inputs of weather observation data provided by the Air Force's ETAC (Environmental Technical Applications Center) database of airport weather observations. Certain sites do not make weather observations at night if no aircraft are scheduled to land. Six hours is about the longest gap permissable without incurring significant estimation errors. As should be obvious, the TGRAD model is not predictive in the temporal sense. That is, it cannot operate without a continuous input of observed station data. Rather, it is designed to fill in knowledge gaps concerning the vertical structure of the surface layer using the measurements from a single tower level and some indication of initial soil characteristics. However, if a synoptic estimation of the predicted weather were available (temperature, winds, relative humidity, and cloud cover as functions of time), estimates of surface layer flux and vertical structures could be predicted, based on the outcomes of the higher level model.

TABLE 1. SYMBOL TABLE FOR SUBROUTINE TGRAD

Name	Type	Location	Description
AA, AAA	Real	Local	Coefficients of sensible heat
AB1, AB2	Real	Local	Coefficients used in foliage temperature calculations
ALBEDO	Real	Local	Original soil albedo
ALPHAF	Real	Local	Foliage albedo
ALPHAG	Real	Local	Soil albedo with variable moisture content
ALPHAP	Real	Local	Fractional surface moisture
ANUM	Double	Local	Numerator of ground temperature equation
BB, BBB	Real	Local	Coefficients of latent heat
BETA	Real	Local	Constant in turbulence equations
BG	Real	Local	Fractional amount of bare ground
C1, C2	Real	Local	Constants used in force-restore rate equation for ground surface temperature
CC1, CC2	Real	Local	Coefficients in the rate equation for ground surface moisture
CCV(3)	Real	Common	Cloud fractions for three cloud layers: 1-highest, 2-middle, 3-lowest
CDEGK	Double	Local	Conversion from Celsius to Kelvin
COSZ	Real	Local	Cosine of the solar zenith angle
CP	Real	Local	Specific heat of air at constant pressure
D1	Real	Local	Soil depth influenced by the diurnal temperature cycle, equal to SQRT(THERDF*TAU1)
D12, D1G	Real	Local	Values of D1 with moisture added
D1P	Real	Local	Soil depth (0.1m) influenced by the soil moisture cycle
D2	Real	Local	Soil depth influenced by the annual temperature cycle, equal to 19.1×D1

Name	Type	Location	Description
D2P	Real	Local	Soil depth (0.5m) influenced by the seasonal moisture variations
DBARD2	Real	Local	Earth-sun distance modification factor
DEC	Real	Local	Declination of the sun in radians
DELC	Real	Local	Step function, equal to 1, except during condensation
DELLNG	Real	Common	Difference between the local longitude and the time zone meridian (west > 0)
DELTXK	Real	Local	Diffence between TEFF and TG × K
DENOM	Double	Local	Denominator of ground temperature equation
DLAT	Real	Common	Local latitude in degrees (30.5 is 30° 30')
DQSGDT	Real	Local	Derivative of QSG with respect to TG
DT	Real	Local	Time increment in seconds
DTDZ	Real	Common	Temperature gradient
EF	Real	Local	Evaporation rate from foliage
EFFALB	Real	Local	Ground-foliage effective albedo
EFPOT	Real	Local	Potential evaporation rate from foliage
EG	Real	Local	Evaporation rate at ground surface
EH	Real	Local	Evaporation rate just above foliage canopy
EMF	Real	Local	Foliage emissivity
EMG	Real	Local	Ground surface emissivity
ETR	Real	Local	Transpiration rate
FC	Real	Local	Fractional foliage cover
G1,2,3,4	Real	Local	Sets of values used more than once
HA	Real	Local	Sum of fluxes to atmosphere (positive when directed upward)
HETCAP	Real	Local	Heat capacity of soil
HRANGL	Real	Local	Hour angle of sun in radians

Name	Type	Location	Description
HSF	Real	Local	Sensible heat flux from foliage (positive when directed upward)
HSG	Real	Local	Sensible heat flux from ground surface
HSH	Real	Common	Sensible heat just above foliage canopy
ICL	Integer	Common	Cloud types coding flag
IGAP	Integer	Common	Flag to reinitialize after gaps in data
ISOIL	Integer	Local	Soil type local to TGRAD (can be changed)
ISOILO	Integer	Local	Previous soil type
ISUNRS	Integer	Common	Time of local sunrise in minutes from midnight
ISUNST	Integer	Common	Time of local sunset in minutes from midnight
ITG	Integer	Common	Flag for using measured ground temperature
IYR	Integer	Common	Last two digits of the year
JD	Integer	Common	Julian date
JDO	Integer	Local	Previous Julian date
JSOIL	Integer	Common	Initial soil type
K	Real	Local	Von Kármán's constant
L	Real	Local	Latent heat of vaporization
LAM2	Real	Local	Thermal conductivity of deep soil
LAMG	Real	Local	Thermal conductivity of top soil
LAMGO	Real	Local	Initial thermal conductivity of soil
LF	Real	Local	Latent heat of fusion
MIN	Integer	Common	The current minute of the day from midnight
MINDEL	Integer	Common	Time increment in minutes
N	Real	Local	Net leaf area index
OBUKLN	Real	Common	Monin-Obukhov length
ONE3RD	Double	Local	Constant equal to one-third

Name	Type	Location	Description
P1	Real	Local	Value multiplied by HA in force restore equation for ground temperature (D-8a)
P2	Real	Local	Value multiplied by (TG-T2) in same equation
PC2	Real	Local	Heat capacity of deep soil
PCG	Real	Local	Heat capacity of top soil
PG	Real	Local	Precipitation rate felt at ground surface
PI	Real	Local	Constant equal to π
PRECIP	Real	Common	Precipitation rate
PRES	Real	Common	Atmospheric pressure in millibars
PSCSD1	Real	Local	Heat capacity times thermal diffusivity for top soil
PSCSD2	Real	Local	Heat capacity times thermal diffusivity for deep soil
QA	Real	Local	Specific humidity of the air
QDUM	Real	Local	Dummy variable used in subroutine call
QSA	Real	Local	Saturated specific humidity of the air
QSF	Real	Local	Saturated specific humidity of the foliage
QSG	Real	Local	Saturated specific humidity of the ground
RA	Real	Local	Aerodynamic resistance (returned from CN)
RAIR	Real	Local	Gas constant for air
RH	Real	Common	Relative humidity (not in percent)
RHOA	Real	Local	Density of the air
RHOW	Real	Local	Density of water
RL	Real	Local	Longwave radiative flux from the atmosphere
RLAT	Real	Local	Local latitude in radians
RLG1,2	Real	Local	Sets of values of RL used more than once
RP	Real	Local	Soil moisture interpolation factor
RPP	Real	Local	Fraction of potential evaporation rate from foliage

Name	Type	Location	Description
RS	Real	Local	Generalized stomatal resistance
SO	Real	Local	Maximum incident solar radiation
SDN	Real	Common	Incident solar radiation at the ground surface
SGHEAT	Real	Local	Net solar radiative flux
SIG	Real	Local	Stefan-Boltzman constant
SMAX	Real	Local	Maximum solar radiation at local noon
SOIL(9,6)	Real	Local	Sets of soil parameters
SOLMAX	Real	Local	Solar constant
SS	Real	Local	Seasonal dependence of stomatal resistance
T2	Double	Local	Temperature of the soil over depth D2 in Kelvin
T2C	Real	Common	Same as T2 in ° Celsius
TAC	Real	Common	Air temperature at reference height in ° Celsius
TAIR	Double	Local	Air temperature at reference height in Kelvin
TAU1	Real	Local	Diurnal period in seconds
TCCV	Real	Common	Total fraction of cloud cover
TEFF	Double	Local	Ground surface/foliage effective temperature
TF	Double	Local	Average foliage temperature in Kelvin
TFC	Real	Common	Average foliage temperature in ° Celsius
TG	Double	Local	Ground surface temperature in Kelvin
TGC	Real	Common	Ground surface temperature in ° Celsius
THERDF	Real	Local	Thermal diffusivity of soil
TNOON	Real	Local	Time of local noon in minutes from midnight
TSTAR	Real	Local	Virtual temperature in Kelvin
TUA	Double	Local	Upper air temperature in Kelvin
USTAR	Real	Common	Friction velocity
VPA	Real	Local	Vapor pressure of the air in millibars

Name	Type	Location	Description
VPDUM	Real	Local	Dummy variable used in subroutine call
W2	Double	Local	Dimensionless volumetric concentration of soil moisture over depth D2
W20	Double	Local	Initial value of W2
WD	Double	Local	Mass of liquid water retained by foliage per unit horizontal ground area
WDMAX	Double	Local	Maximum value of WD beyond which runoff to the ground occurs
WG	Double	Local	Same as W2 for top soil
WG0	Double	Local	Initial value of WG
WIND	Real	Common	Windspeed at reference height
WK	Double	Local	Critical or saturated value of WG
WMAX	Real	Local	Maximum value of WG
WMIN	Real	Local	Minimum value of WG
WS	Real	Local	0.9W2 + 0.1WG
WWILT	Real	Local	Wilting point value of WG
Z	Real	Common	Desired height for temperature gradient
Z0	Real	Common	Roughness height of the terrain

TABLE 2. INPUTS TO SUBROUTINE TGRAD

Name	Description *-indicates the value has been preset within the subroutine
IYR	Year used in calculating solar declination.
JD	Julian date.
JSOIL,SOIL*	JSOIL indicates soil type, SOIL is an array containing values of soil characteristics arranged by soil type. The following are elements of SOIL.
SOIL(1,*)*	Ground surface emissivity. Set to EMG in main routine.
SOIL(2,*)*	ALBEDO of the surface.
SOIL(3,*)*	THERDF (thermal diffusivity) of the ground.
SOIL(4,*)*	HETCAP (heat capacity) of the ground.
SOIL(5,*)*	WGO, the initial fractional water content, by volume, of the first 10 cm of soil.
SOIL(6,*)*	WK, the fractional water content, by volume, at which the soil acts as if saturated.
SOIL(7,*)*	W20, the initial fractional water content, by volume, of the first 50 cm of soil. The value of WGO is subsumed within this value.
SOIL(8,*)*	WWILT, is a measure of the resistance of foliage to evaporative processes as the soil becomes drier.
SOIL(9,*)*	WMIN, the minimum value allowed for the soil moisture. If no minimum was given, the calculation of WS could reach zero and the stomatal resistance equation would approach infinity.
MIN	The driver routine accounts for time and reads data from an external source on an hourly to 3 hourly basis. MIN is the minutes past midnight in local standard time.
MINDEL	Time increment between successive surface energy budget calculations. A standard value of 10 minutes has been chosen.
ITG	ITG flags whether or not user wants to input soil temperature.

Name	Description
IGAP	IGAP is a driver flag indicating that the time since the last data set was too long to be relevant. Parameters are reinitialized as at the start of the program.
ISOILO	ISOILO is the initial soil type; provision is made within TGRAD to vary the soil type by season, so in cases of reinitialization, the original soil parameters can be recalled if needed.
ICL	Cloud type category, as listed in the CLOUD subroutine.
PRES	Measured pressure, in millibars.
RH	Measured relative humidity.
WIND	Measured windspeeds converted to meters per second.
CCV(3)	Cloud cover amounts in three cloud height categories: low, medium, and high. Only occasionally are three layers of data available.
TCCV	Total fractional cloud cover.
DLAT	Latitude of site chosen.
AFC	The original fractional foliage cover value, used when reinitializing.
ZO	Surface roughness length.
DELLNG	DELLNG is the difference in longitude between the site's longitude and the meridian used as a basis of time. For example, WSMR is located at approximately 106° W longitude. It's DELLNG would be +1°. A location in the eastern hemisphere, at 106° E would have a DELLNG of -1°. This convention is used to calculate the exact time of sunrise and sunset for each location.
Z	Height desired for temperature gradient calculation. According to similarity theory, knowledge of certain scaling parameters allows one to calculate the gradient anywhere within the boundary layer.
PRECIP	Precipitation rate in kg/s-m^2.
TAC	Measured station temperature in ° Celsius.
TGC	Ground temperature in ° Celsius. While usually calculated within the model, it can also be entered as a program input variable.

Name	Description
K*	Von Karman's constant, a similarity theory constant equal to 0.4.
ALPHAF*	Albedo of the foliage, set to 0.2.
EMF*	Emissivity of the foliage. Albedo is a general reflectivity to the solar radiation spectrum, and emissivity is the generalized ability of a surface to emit energy in the infrared spectrum through 'graybody' radiation.
SOLMAX*	The solar constant of 1369.2 W/m^2 at the Earth's orbit radius.
ALBSNO*	Albedo of a typical snow cover, set at 0.6.
BETA*	A similarity constant used for nocturnal boundary layer characterization. In the literature β varies between approximately 4.7 and 9.5.

The soil parameters are declared in the BLOCK DATA segment of the code. Deardorff (1978) listed 5 sets of soil parameters in his paper. Other sets were found in Oke (1978). These latter sets had separate categories for dry and wet soil types, while Deardorff had simple parameterizations of albedo, heat capacity, and thermal conductivity to account for variations in soil moisture. Deardorff's equations were adopted as equations (54a) through (54c), except that (54b) has been correctly modeled by including the $w_{max}^{1/3}$ factor in the denominator. A comparison between Deardorff's soils and Oke's soils shows they are virtually the same soil types when moisture differences are taken into account. The values of w_k and w_{wilt} were taken from a chart found on page 42 of Oke (1978). Soil types include clay, snow, a "wet" desert sand (steppe), and a dry desert sand. Alternatively, different soil parameters could be read in for the location, but this would require a change in the parameters passed through the unnamed common block.

3.2 CN

Subroutine CN uses the theory in section 2.1.4 to calculate various flux-profile parameters, including the Obukhov length, OBUKLN; the friction velocity, USTAR; and the dimensionless temperature gradient function, PHIH. From these quantities the sensible heat flux and the other propagation related parameters discussed in section 2.4 can be calculated. In the program, equations derived from Thom's work are designated with a T. The basic flux-profile equations are those obtained from Hanna *et al.* (1982). These equations are designated with an H, though several other authors have identical equations.* Table 3 shows the names and short descriptions of all the variables used in subroutine CN.

*Also, for lack of characters at least one variable needed to be renamed. r_H, the atmospheric resistance term, is expressed as RA, while R_H, the relative humidity is expressed as RH.

TABLE 3. SYMBOL TABLE FOR SUBROUTINE CN

Name	Type	Location	Description
BH	Real	Local	Excess of resistance due to heat flux
CHANGE	Real	Local	Relative change in USTAR iterations
CON	Real	Local	A group of constants
DELZ	Real	Local	Desired height (Z) - roughness height (Z0)
DELZS	Real	Local	Reference height (STAHT) - roughness height
DPTDZ	Real	Local	Potential temperature gradient
HS	Real	Local	Sensible heat flux/(RHOA*CP)
I1	Integer	Local	DO loop counter
KH	Real	Local	Eddy diffusivity for heat
OBMIN	Real	Local	Minimum value of OBUKLN used at night
PHIH	Real	Local	Dimensionless temperature gradient
PHIHMX	Real	Local	Maximum allowed value of PHIH at night
PHIM	Real	Local	Dimensionless wind gradient
POW	Real	Local	Exponent used in conversion from potential temperature to temperature
PSI	Real	Local	The result of integrating PHIM
STAHT	Real	Local	Reference height for air temperature and windspeed measurements
UST	Real	Local	Previous value of USTAR
USTMIN	Real	Local	Minimum value of USTAR used at night

3.3 CLOUD

Subroutine CLOUD was drawn almost verbatim from Shapiro's (1982) three layer cloud model. This is an empirical model based on statistical averages only. Averages represent mean incident radiation from the sun arriving at the surface of the earth. These mean results average out the fluctuations that would occur when direct sunlight hits the surface

on a cloudy day versus when direct sunlight is obscured by clouds. Therefore the results of the model equate to an area average rather than a point calculation.

The parameters brought into the subroutine include the cosine of the zenith angle (COSZ), the solar constant (SO), and the effective albedo (equation (15a)) of the foliage/ground surface. The fractional amounts of clouds in the three layers and their types are passed via the unnamed common. The only output from the routine is the incident shortwave flux at the ground. This result does not distinguish between direct and diffuse radiation.

Table 4 is a listing of the parameters used in the subroutine.

The variable ICLOUD used in the subroutine is a coded number used to denote the cloud types in each of the three layers. This is accomplished by designating individual digits of a five digit number to zeros, ones, or twos. Each digit characterizes one of the three cloud layers or designates a rain or fog condition. In layer one, there is a distinction made between thick cirrus/cirrostratus (Ci/Cs) and thin. Layer two does not distinguish between alto-type clouds. Layer three distinguishes between stratus and cumulus types and also allows for fog and/or smoke. Rain is denoted by overcast conditions in all layers and thick Ci/Cs in layer one. The fractional amounts of cloud type by layer are given in CCV(3) and are reassigned to F1, F2, and F3 within the subroutine. Normally only one cloud type is set in this integer because the input data available usually does not specify cloud type. However, inclusion of a cloud type is a simple addition.

Except for the following notational departures, Shapiro's (1982) work was faithfully reproduced. The overcast coefficients are denoted by P (instead of RHO) and U (instead of TAU), and one character is used for Shapiro's lower-case variable names, and two characters are used for Shapiro's upper-case variable names. The reader interested in more detail regarding Shapiro's model is urged to obtain his report. His methodology and findings will not be repeated here.

TABLE 4. SYMBOL TABLE FOR SUBROUTINE CLOUD

Name	Type	Location	Description
BH	Real	Local	Excess of resistance due to heat flux
D1,2,3	Real	Local	d1, d2, d3 from Shapiro
DD1,2	Real	Local	D1 and D2 from Shapiro
F1,2,3	Real	Local	Same as CCV(3) above
ICLOUD	Integer	Local	Same as ICL above
ID2,3	Integer	Local	Flags for using diffuse values for layers 2 and 3
IPU1,3	Integer	Local	Flags for type of cloud to use in layers 1 and 3
IRAIN	Integer	Local	Flag for rain
IRT3	Integer	Local	Flag for fog and/or smoke present in layer 3
P1,2,3	Real	Local	Overcast reflectivities for 3 layers
PHI1,2,3	Real	Local	Weighting functions for 3 layers
R1,2,3	Real	Local	Clear air reflectivities for 3 layers
RG	Real	Formal	Ground surface-foliage albedo
RR1,2,3	Real	Local	Total reflectivities for 3 layers
T1,2,3	Real	Local	Clear air transmissivities for 3 layers
TT1,2,3	Real	Local	Total transmissivities for 3 layers
U1,2,3	Real	Local	Overcast transmissivities for 3 layers
W1,2,3	Real	Local	Weighting functions for 3 layers
X0	Real	Local	Incident solar radiation above clouds
X3	Real	Formal	Incident solar radiation at ground surface

3.4 TFOL

The computation of the foliage temperature is accomplished in subroutine TFOL using the iterative Newton-Raphson procedure described in section 2.2. Newton's method is the fastest method for solving a polynomial, as long as the first estimate is reasonably close to the solution. This is virtually assured by the small change expected in foliage temperature between timesteps. Table 5 itemizes the variables used in this subroutine.

TABLE 5. SYMBOL TABLE FOR SUBROUTINE TFOL

Name	Type	Location	Description
CHANGE	Double	Local	Relative change of TF after iteration
DQSFDT	Real	Local	Derivative of saturated specific humidity of foliage with respect to TF
FOFTF	Double	Local	F(TF)
FPOFTF	Double	Local	F'(TF)
I	Integer	Local	DO loop counter
QDUM	Real	Local	Dummy variable used in subroutine call
VPDUM	Real	Local	Dummy variable used in subroutine call

In each iterative step, the saturated specific humidity of the foliage and its derivative are found by calling subroutine SPEHU. Then FOFTF (meaning the function F of θ_f) and FPOFTF (F' in equation (47)) are found and the change in TF (θ_f) is found. TF is changed by this amount and a check is made on the amount of the change. A decision was made to exit the subroutine when the change is less than 10^{-4} K. If convergence does not occur within 20 iterations, the program writes an error message along with the last value of TF. The program has never encountered a problem attempting to estimate θ_f.

3.5 SUN

Subroutine SUN finds the times of local sunrise, sunset, and noon (sun directly south) as well as the solar declination. It requires the Julian date (JD), the latitude in radians (RLAT), and the difference in degrees between the location and the standard meridian used for the local time (DELLNG). The latitude enters TGRAD through the unnamed common as DLAT (the latitude in degrees). Then, RLAT is calculated and passed from TGRAD to SUN. Both DLAT and DELLNG are in decimal degrees. The subroutine is used to compute equations (7) through (12), which are used to set up equation (14), the equation for the zenith angle. Table 6 is a compendium of the different variables used in subroutine SUN.

TABLE 6. SYMBOL TABLE FOR SUBROUTINE SUN

Name	Type	Location	Description
ANOON	Real	Local	Solar angle at local noon
BETA	Real	Local	Definition of angle of sunrise or sunset
EOT	Real	Local	Value from equation of time
HRANGL	Real	Local	Hour angle of the sun
SBETA	Real	Local	SIN(BETA)

3.6 SPEHU

Subroutine SPEHU takes a temperature, a relative humidity, and the local pressure and calculates vapor pressure, specific humidity, saturated specific humidity, and the derivative of the saturated specific humidity. There are a total of three calls to this routine: two from TGRAD and one from TFOL.

Equations from Haurwitz (1941) were used, but these equations can be found in most meteorological texts. The derivative of the saturated specific humidity with respect to temperature is a straight forward differentiation, performed in appendix A.

TABLE 7. SYMBOL TABLE FOR SUBROUTINE SPEHU

Name	Type	Location	Description
DQSDT	Real	Formal	Derivative of the saturated specific humidity with respect to the temperature
POW	Real	Local	Exponent used in vapor pressure equation
Q	Real	Formal	Specific humidity
QS	Real	Formal	Saturated specific humidity
TC	Real	Formal	Temperature in ° Celsius
VP	Real	Formal	Vapor pressure
VPS	Real	Local	Saturated vapor pressure

4. SAMPLE DRIVER

As noted, subroutine TGRAD is called by a driver. It was written this way to accommodate differences in the formats of various meteorological data bases. Originally, the Kunkel code was modified to deal with two different sources of data, but even further applications were found to be possible in the modular form adopted. The sole changes required were in the driver. Generally this is true, and since a user will likely have a unique application and data source, the driver listed as figure 3 will serve as a model for a variety of applications.

Figure 4 shows a sample data file. The data was made available from meteorological observations taken at C Station, White Sands Missile Range, New Mexico. Windspeeds recorded as zeros were adjusted upwards by 0.5 m/s to avoid computational errors within the CN subroutine. The Julian date refers to 2 November 1984. When running the program, it will be necessary to remove the first line from the following table. The header line is provided as a simplifying reference to the necessary inputs.

5. MODEL PERFORMANCE AND SENSITIVITY ANALYSIS

The performance of the TGRAD model has been evaluated twice. First, Kunkel (1985) evaluated the ability of the model to estimate the vertical temperature gradient. Then Tofsted and Gillespie (1986) compared the model performance with the Deardorff model and an improved version of TGRAD, which we shall call TGRAD 2.0. Kunkel's analysis was the motivation for TGRAD 2.0, since his analysis uncovered two areas where TGRAD performed below expectations. The first area was in regard to using a surface-energy-budget-driven near-surface air temperature. As indicated in section 2.1, this modification has been included in this version of the model. A second area was model performance for snow-covered terrain. A follow-on version of TGRAD, called TGGEN, attempted to account for this effect through inclusion of melting effects. However, a decision was made to document the TGRAD model without describing the snow interaction effects since the major portion of the model has not changed and because the amount of description required to explain the snow-cover effects is rather large and best left to a separate discussion.

Kunkel's other basic findings related to the direct components in the equation computing temperature gradient. These factors were: the degree of accuracy in the measurement of windspeed and temperature, the model's method used in estimating sensible heat, error in estimating the roughness length at the site, and differences in the theoretical functional form for the ϕ_h term. He found first that the measurement of temperature was unimportant. Second, he determined that changes in the roughness length of 50 percent only produced gradient changes up to 16 percent, indicating relative model insensitivity to large errors in estimating the roughness length. Third, he analyzed the ability of the model to estimate the sensible heat flux. He found the model does a reasonable job for a variety of different surface types. His table was left out of the proceedings of his EOSAEL conference paper, so it is included here as table 8.*

---

* As Kunkel notes, the values available in the literature are few, and, in general, insufficient information is provided with the sensible heat flux values to be able to accurately use the model. For this reason Kunkel ran the model with a range of inputs in order to bracket the possible conditions present when the cited flux values occurred.

```
      PROGRAM TGS !1000 <860203.0926>
C
C     DRIVER PROGRAM FOR TGRAD SURFACE ENERGY BUDGET MODEL
C
      INTEGER PP(5)
      REAL*8 WG,WMAX
      COMMON JYR,JD,JSOIL,JMIN,JMINDEL,JTG,JGAP,JSUNRS,JSUNST,ISOIL0,
     1 JCL,PRES,RH,WIND,CCV(3),TCCV,DLAT,DELLNG,AFC,Z0,Z,PRECIP,DTDZ,
     2 SDN,HSH,TAC,TGC,TFC,T2C,USTAR,OBUKLN,WG,WMAX,CN2
C
C        PP(1) IS THE ENDING MINUTE FROM MIDNIGHT OF THE JULIAN DATE
C              FROM UNIT 4; CAN BE GREATER THAN 1440.
C        PP(2) IS THE OUTPUT INTERVAL FOR UNITS 9 AND 10.
C        PP(3) IS THE STARTING MINUTE FROM MIDNIGHT OF THE JULIAN DATE
C              FROM UNIT 4.
C        PP(4) IS EITHER THE VALUE OF THE TIME INTERVAL USED IN TGRAD,
C              (ALLOWABLE VALUES: 1-10), OR THE VALUE OF THE RANGE IN
C              THE MISS DISTANCE CALCULATIONS (ALLOWABLE VALUES: >500 M).
C        PP(5) IS A FLAG FOR USING THE MEASURED GROUND TEMPS;
C              DEFAULT IS OFF.
C
      CALL RMPAR(PP)
C     1440 30 0 10 0
      INT=PP(2)
      IF(PP(2).LE.0)INT=1
      IEND=PP(1)
      IF(IEND.LE.1)IEND=32767
      ISTART=PP(3)
      IF(ISTART.LT.0)ISTART=1440+ISTART
      ISTART=MOD(ISTART,1440)
      ADT=0.0
      JMINDEL=10
      RANGE=1000.0
      IF(PP(4).GE.500)RANGE=PP(4)
      JTG=PP(5)
      JSTAT=0
      WRITE(9,700)'TGRAD RESULTS'
 700  FORMAT(///////A13/)
      REWIND 4
      REWIND 8
      JGAP=0
      IBAD=0
      JMIN=ISTART
C
C   READ IN LOCATION PARAMETERS; MORE THAN ONE SET CAN BE USED FOR
C   THE SAME MET DATA.
C
      READ(4,*)JD0,AFC,Z,Z0,DLAT,DELLNG,ICLOUD,JSOIL,JYR,PRETRG
      JD=JD0
      WRITE(7,*)JD,AFC,Z,Z0,DLAT,DELLNG,ICLOUD,JSOIL,JYR,IWHICH
      GO TO 100
C
C
  20  IF(MOD(JMIN+1440,JMINDEL).NE.0)GO TO 100
      IF(JGAP.EQ.0.OR.JTG.EQ.2)TGC=ATG
      PRECIP=0.0
      IF(TAC.LE.PRETRG)PRECIP=2.77778E-4
      IF(JGAP.EQ.0)THEN
C
C** NEW DAY:  BEGINNING OF DATA OR GAP IN DATA; INITIALIZE **
C
        WRITE(7,600)
 600    FORMAT('NEW DAY')
        PI=3.14159
        RLAT=DLAT*PI/180.0
        CALL SUN(PI,RLAT,DEC,TNOON)
        ITIM1=JSUNRS/60*100+MOD(JSUNRS,60)
        ITIM2=JSUNST/60*100+MOD(JSUNST,60)
        WRITE(9,*)'SUNRISE=',ITIM1,' SUNSET=',ITIM2
        WRITE(9,690)'  JD  MIN  WIND TCCV DTDZ CN2    L     TG',
     1            '   TF   TA    SDN  W2/WMAX   IG   SNOW',
     2            '    HSH  MISSD  RADBAL'
 690    FORMAT(/A41,A38,A22/)
        JD1=JD
        ENDIF
C
C     NEW JULIAN DATE
C
      IF(JD.NE.JD0)THEN
        JD0=JD
        ITIM1=JSUNRS/60*100+MOD(JSUNRS,60)
        ITIM2=JSUNST/60*100+MOD(JSUNST,60)
        WRITE(9,*)'SUNRISE=',ITIM1,' SUNSET=',ITIM2
        ENDIF
```

Figure 3. Simplified driver program TGS.

```
C
C
      CALL TGRAD(JSTAT,WGARF,AIS,RADB)
      AMISSC=7.75E-5*PRES/(TAC+273.16)**2*DTDZ*RANGE*RANGE/2.0
      IF(MOD(JMIN+1440,INT).EQ.0)THEN
        WRITE(9,650)JD,JMIN,WIND,TCCV,DTDZ,CN2,OBUKLN,
     1              TGC,TFC,TAC,SDN,10000.*WGARF,HSH,AMISSC,RADB
  650   FORMAT(I4,I5,F6.2,F4.1,F5.2,F6.2,F7.0,3F5.1,F6.1,F9.4,12X,
     1         F9.4,F7.3,F7.2)
        ENDIF
      JMIN=JMIN+JMINDEL
      IF(JMIN.EQ.(IEND+JMINDEL))GOTO 80
      IF(IFBRK(IDUM))80,70 !1000
   70 IF(MOD(JMIN,INT).EQ.0)GO TO 100
      IF((JD-JD1)*1440+JMIN.LT.IEND)GO TO 20
  100 READ(8,*)ID,IT,PRES,TAC,RH,WIND,TCCV
      WRITE(7,*)JD0,JD,ID,IT,PRES,TAC,RH,WIND,TCCV
      IF(ID.GT.JD)THEN
        JMIN=0
        JD=ID
        ENDIF
      IF(WIND.LT.0.5)WIND=0.5
      IF(RH.LT.1.0)RH=RH*100.0
      RH=RH/100.0
      JCL=01111
      IF(ICLOUD.EQ.2)JCL=02111
      IF(ICLOUD.EQ.5)JCL=01121
      IF(ICLOUD.EQ.6)JCL=01112
      IF(ICLOUD.EQ.7)JCL=12111
      CCV(1)=0.0
      CCV(2)=0.0
      CCV(3)=0.0
      IF(ICLOUD.LE.2)CCV(1)=TCCV
      IF(ICLOUD.EQ.3)CCV(2)=TCCV
      IF(ICLOUD.EQ.4.OR.ICLOUD.EQ.5)CCV(3)=TCCV
      GO TO 20
C
C   AT END OF FILE OR JD IS 0
C
   80 STOP
      END
```

Figure 3. (cont) Simplified driver program TGS.

As discussed above and as seen in table 8, the model does not do well in estimating sensible heat flux in the warm-advection-over-snow case. The estimation of roughness length and differences in form for the ϕ_h function were the most significant sources of error for this case.

Kunkel also found that a 15 percent error in measurement of the windspeed caused at least a 15 percent change in the estimated temperature gradient at night. The change was greatest for windspeeds of 2 m/s where the variation was 24 percent. Windspeeds of this velocity are common for highly stable episodes, and thus windspeed can be a critical parameter in estimation of the nocturnal flux cases.

In regard to Kunkel's investigation of the effects of variations in the functional forms for ϕ_h, Yaglom (1977) provided a compendium of various functional forms proposed by researchers in this area. Apparently, even after twenty years of research in the area, there is no general agreement on the proper form (especially at night). In his analysis, Kunkel ran the model using a range of these proposed form-fit coefficients. The results showed that for the higher windspeeds (between 10 and 15 m/s), the degree of variation of the results about the standard model were 12 percent during the day and 17 percent at night. At 6 m/s the variations were 20 percent during the day and 15 percent at night. At 2 m/s the variations were 45 percent during the day and 57 percent at night. Apparently then, the largest source of error is due to the functional form used for the dimensionless temperature gradient. The best functional form and related coefficients to address this problem are still not known. Numerous investigators have been tackling this problem for the past

JULD	TIME	PRES	TEMP	RH	WIND	CLCV
226	0	880.0	17.90	73.0	1.1	0.00
226	30	880.0	18.18	71.0	1.1	0.00
226	60	880.0	18.25	70.0	1.1	0.00
226	90	880.0	17.10	72.0	1.1	0.00
226	120	880.0	17.24	76.0	0.9	0.00
226	150	880.0	17.43	74.0	0.9	0.00
226	180	880.0	16.29	76.0	1.6	0.00
226	210	880.0	15.47	75.0	1.5	0.00
226	240	880.0	15.99	73.0	1.6	0.00
226	270	880.0	16.79	72.0	1.3	0.00
226	300	880.0	16.20	71.0	1.2	0.00
226	330	880.0	15.44	76.0	1.3	0.00
226	360	880.0	16.69	74.0	1.1	0.00
226	390	880.0	17.96	70.0	1.4	0.00
226	420	880.0	20.17	59.0	1.8	0.00
226	450	880.0	21.71	52.0	1.6	0.00
226	480	880.0	23.26	46.0	1.0	0.00
226	510	880.0	24.73	40.0	0.8	0.00
226	540	880.0	24.87	39.0	1.4	0.00
226	570	880.0	25.88	38.0	2.1	0.00
226	600	880.0	28.75	33.0	1.7	0.00
226	630	880.0	30.32	26.0	1.5	0.00
226	660	880.0	32.38	21.0	1.7	0.00
226	690	880.0	33.25	18.0	2.3	0.00
226	720	880.0	31.91	15.0	2.3	0.00
226	750	880.0	34.27	14.0	2.8	0.00
226	780	880.0	33.38	12.0	2.8	0.00
226	810	880.0	33.01	12.0	4.5	0.00
226	840	880.0	32.85	11.0	4.3	0.00
226	870	880.0	33.14	11.0	3.8	0.00
226	900	880.0	33.19	11.0	3.8	0.00
226	930	880.0	33.11	11.0	3.6	0.00
226	960	880.0	32.97	11.0	4.1	0.00
226	990	880.0	32.70	11.0	3.9	0.00
226	1020	880.0	32.55	12.0	3.9	0.00
226	1050	880.0	31.71	12.0	4.3	0.00
226	1080	880.0	30.54	13.0	3.2	0.00
226	1110	880.0	28.90	16.0	2.3	0.00
226	1140	880.0	26.66	20.0	1.6	0.00
226	1170	880.0	25.13	27.0	1.4	0.00
226	1200	880.0	24.30	32.0	1.6	0.00
226	1230	880.0	22.71	36.0	1.7	0.00
226	1260	880.0	20.99	40.0	1.6	0.00
226	1290	880.0	19.71	47.0	1.5	0.00
226	1320	880.0	20.07	45.0	1.5	0.00
226	1350	880.0	19.29	43.0	1.4	0.00
226	1380	880.0	18.12	49.0	0.7	0.00
226	1410	880.0	16.39	62.0	0.7	0.00
226	1440	880.0	17.04	64.0	1.0	0.00

Figure 4. Sample data set.

TABLE 8. COMPARISON OF MODELED SENSIBLE HEATS WITH LITERATURE DERIVED VALUES
(units of W/m^2)

	Midday		Night	
Surface Type	Model	Literature	Model	Literature
Snow	75-125	100	-15	-5
Snow,warm advection	65-100	-50	-13	-100
Wisconsin farm	170-260	130	-31	-30
California farm	169-270	165	not avail.	not avail.
Minnesota farm	120-210	180-220	not avail.	not avail.
Forest	170-270	175	-34	-49
Desert	250-350	252	-32	-35
Clay pasture	180-280	215	not avail.	not avail.

twenty years. The results used in the model are those agreed upon by most investigators, especially the daytime form fit that was thoroughly investigated in the Paulson (1970) paper. The nighttime coefficients are much less universally chosen, and though a β value of 5 was used in the model, a change to 7 or 8 may be warranted (see appendix B).

In Tofsted and Gillespie (1986), TGRAD (original model) was compared with TGRAD 2.0, with the original Deardorff model (here named SURFA), and with measured data. Figures 5 through 10 are reproduced from that paper. In Figure 5 the improvement of both TGRAD and TGRAD 2.0 over SURFA is seen through a comparison of model results of sensible heat flux. This figure shows that instituting the change in near-surface air temperature calculation suggested by Kunkel results in improved sensible heat calculations. Both the original TGRAD and TGRAD 2.0 are superior to SURFA. SURFA results in an overestimate of sensible heat, while simultaneously restricting heat flow in other forms. The surface temperature therefore remains high into the nighttime and results in a positive heat flow at night when the surface temperature should be lower than the air temperature. Figure 6 shows that the net result of the incorrect heat flux calculations of SURFA result in large errors in the temperature gradient estimation. Again, TGRAD and TGRAD 2.0 work nearly identically, with the improved version performing slightly better.

In Figures 7 and 8 the model results are compared with a time history of the refractive index structure parameter. Figure 7 shows the thermal probe data, which normally reads differently than scintillometer data. Figure 8 is based on scintillometer data, and modeled data match it better. Interestingly, though SURFA does poorly in modeling sensible heat flux and temperature gradient, for the Deming data it estimates the turbulence data as well as, if not better than, the other two models estimate the data. But when compared to the White Sands data, the SURFA results are obviously high during the daytime and in the early evening period.

Figures 9 and 10 show results over a vegetated field (in figure 9) and the same field when snow-covered in winter (figure 10). Again SURFA's ability to estimate temperature gradient (figure 9) is below that of either version of TGRAD. In figure 10, SURFA

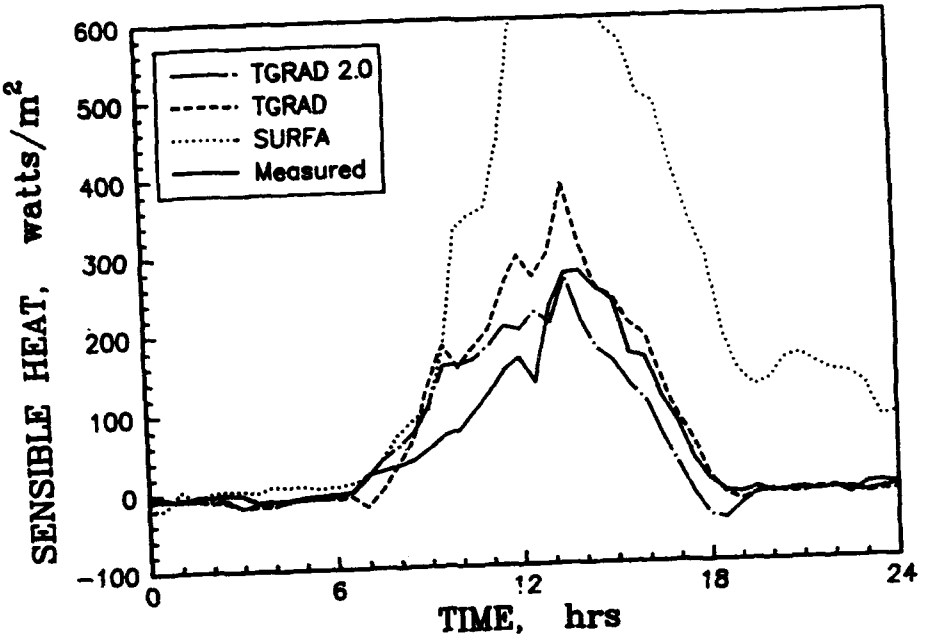

Figure 5. Modeled sensible heats are compared against data measured at Deming, NM, on 14 Aug 1985 over a 15 percent foliage cover of a vineyard.

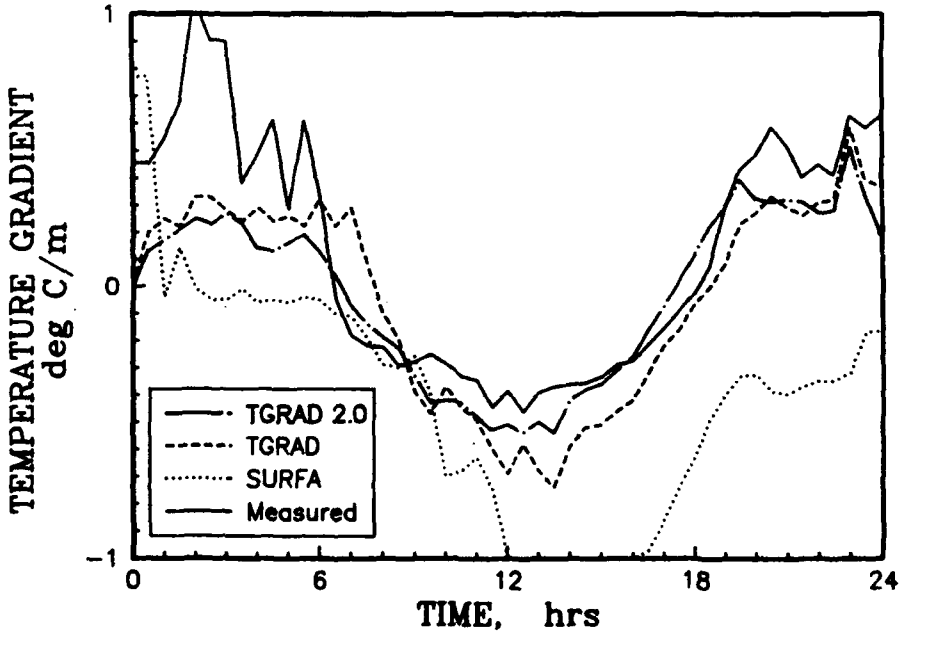

Figure 6. Measured and modeled vertical temperature gradients for the Deming site 14 Aug 85.

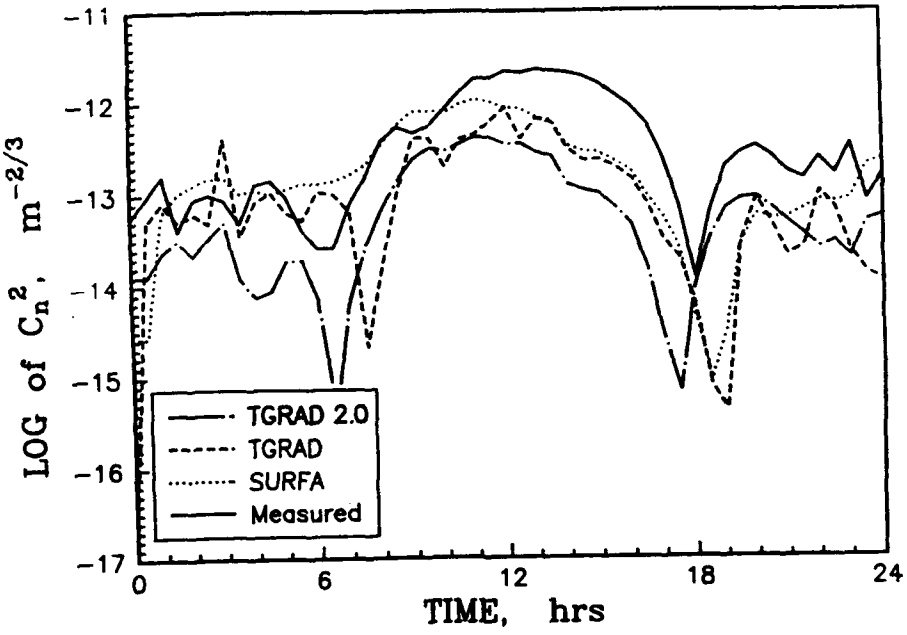

Figure 7. Measured and modeled C_n^2 for the Deming site 14 Aug 85.

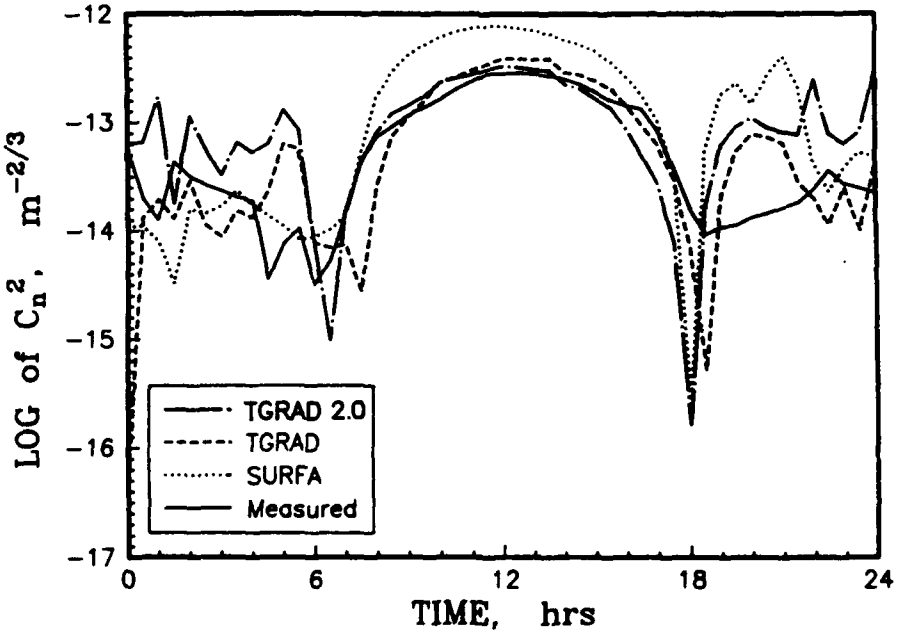

Figure 8. Measured and modeled C_n^2 for WSMR, NM, 15 Jul 84. The surface was nonfoliated.

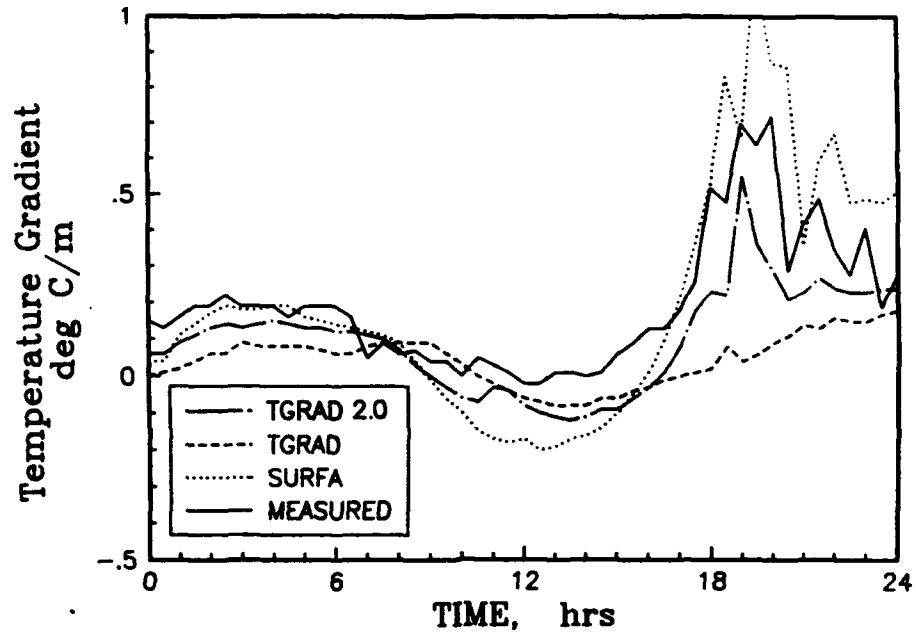

Figure 9. Comparison of measured and modeled temperature gradients for a site near Flatteville, IL, on 24 Jun 1984.

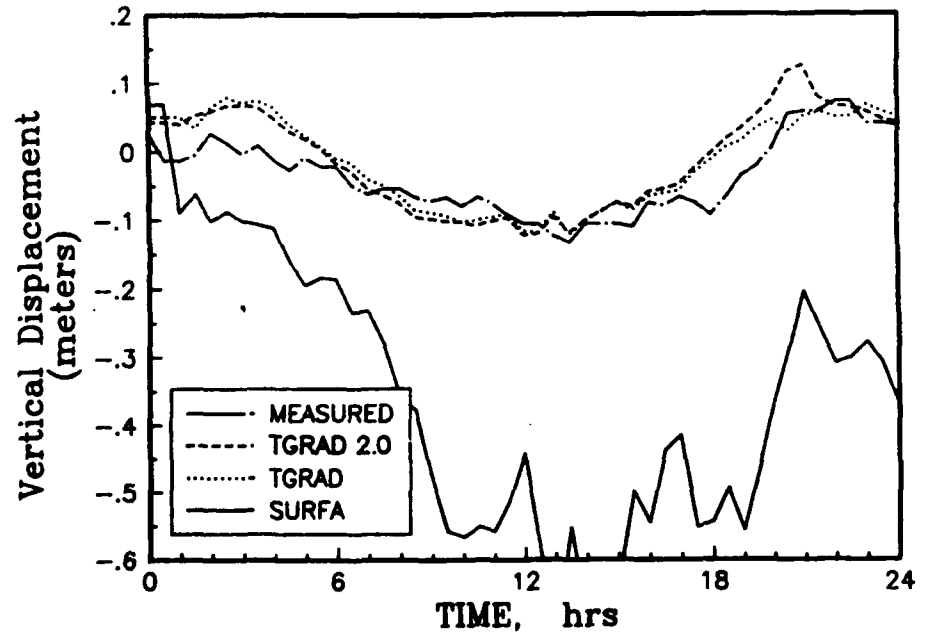

Figure 10. Comparison of measured and modeled temperature gradients for the Flatteville site on 17 Feb 1985.

overestimates the gradient during the evening period because low windspeeds unbalance the equation set used to calculate the flux-profile parameters. However, TGRAD does a good job in approximating the summertime case, but fails in the winter night case — yet for different reasons. First, TGRAD does not use the near-surface air temperature method of TGRAD 2.0. Second, the version of TGRAD 2.0 used in computing this figure allowed the characteristics of the soil to vary as the water froze. With a lower thermal conductivity, the temperature could drop faster, and the gradients increased in magnitude. But even TGRAD 2.0 was incapable of predicting the correct gradients at night, due to the effects of condition (67) and the corresponding need to set u_* to a minimum value to keep the algorithm from yielding negative L values at night.

The case of high temperature gradients at night is equivalent to reaching the critical Richardson number where turbulent motions in the atmosphere are no longer possible. There are several possibilities to dealing with the super-critical-Richardson-number stable case. One method tried has been to scale the gradient upwards based on a functional form related to the amount by which the stability exceeds the critical value. Another method explored would be to find a stochastic set of values of the temperature gradient at night. Therefore, though not predicting an answer, at least a better estimate of actual gradients can be obtained for system performance purposes. A third approach would be similar to the second, but would attempt to catagorize the statistics by timed wave actions within the surface layer. A simulation would therefore entail the setting up of various wave states that have characteristic break times. Each wave would carry a certain amount of the total momentum energy of the surface layer, which would be transfered to the ground in the form of turbulence at the time of the wave break. The net result would be a combination of empirical observations of wave-structure-related-temperature-gradient-variations and a wave model that would start after sunset. Unfortunately, these techniques would not be sufficient to characterize the other meteorological parameters that must be modeled to understand the surface layer atmosphere, but once methods had been developed for one variable, similar approaches could be employed for the others.

6. CONCLUSIONS

The model TGRAD has been shown to provide accurate estimates of daytime surface layer structures for temperature gradient, and, by implication, for other surface layer parameters as well. Baseline estimates are available as functions of the time of day, including nocturnal temperature structure estimates. The model derived is a significant improvement in performance over the previous Deardorff model on which it is based, while retaining the feature of estimating sensible heat flux, taking into account foliage effects. The model is capable of estimating all the flux-profile parameters necessary to calculate the refractive index structure parameter as well as the vertical temperature and wind profiles.

At night, the problem of a highly stable atmosphere is significant, and as yet not completely solved. Methods have been described whereby progress in this area may be made. For now the model described is sufficient to correctly estimate temperature gradients up to about 0.5 °C/m at 2 m a.s.l.

LITERATURE CITED

Allen, L. H., and E. R. Lemon, 1972, "Net Radiation Frequency Distribution in a Corn Crop," *Boundary-Layer Meteorol*, 3:246-254.

Bhumralker, C. M., 1975, "Numerical Experiments on the Computation of Ground Surface Temperature in an Atmospheric General Circulation Model," *J Appl Meteorol*, 14:1246-1258.

Blackadar, A. K., 1976, "Modeling the Nocturnal Boundary Layer," *Proceedings of the Third Symposium on Atmospheric Turbulence, Diffusion and Air Quality*, 46-49, Amer Meteorol. Soc., Boston, MA.

Businger, J. A., 1973, "Turbulent Transfer in the Atmospheric Surface Layer," in *Workshop on Micrometeorology*, D. A. Haugen, ed., American Meteorological Society, 45 Beacon St., Boston, MA 02108

Deardorff, J. W., 1978, "Efficient Prediction of Ground Surface Temperature and Moisture, With Inclusion of a Layer of Vegetation," *J Geophys Res*, 83(C4):1889-1903.

Dyer, A. J., 1974, "A Review of Flux-Profile Relationships," *Boundary-Layer Meteorol*, 7:363-372.

Garratt, J. R., and B. B. Hicks, 1973, "Momentum, Heat and Water Vapour Transfer to and from Natural and Artificial Surfaces," *Q J Roy Meteorol Soc*, 99:680-687.

Halstead, M. H., R. L. Richman, W. Covey, J. D. Merryman, 1957, "A Preliminary Report on the Design of a Computer for Micrometeorology," *J Meteorol*, 14:308-325.

Hanna, S. R., G. A. Briggs, and R. P. Hosker, Jr., 1982, *Handbook on Atmospheric Diffusion*, U. S. Dept. of Energy Technical Information Center, DOE-TIC-11223.

Haurwitz, B., 1941, *Dynamic Meteorology*, McGraw Hill, New York.

Hoffert, M. I., and J. Storch, 1979, "A Scheme for Computing Surface Fluxes From Mean Flow Observations," *Boundary-Layer Meteorol*, 17:429-442.

Jackson, R. D., 1973, "Diurnal Changes in Soil Water Content During Drying," in *Field Soil Water Regime*, pp. 37-55, Soil Science Society of America, Madison, WI.

Kunkel, K. E., and D. L. Walters, 1983, "Modeling the Diurnal Dependence of the Optical Refractive Index Structure Parameter," *J Geophys Res*, 88(C15):10,999-11,004.

Kunkel, K. E., 1985, "Evaluation of a Model for Estimating Vertical Temperature Gradients in the Atmospheric Surface Layer," *Proc 5th Ann EOSAEL/TWI Conf*, US Army Atmospheric Sciences Laboratory, White Sands Missile Range, NM 88002-5501, 138-143.

Lewellen, W. S., 1977, "Use of Invariant Modeling," in *Handbook of Turbulence*, W. Frost and T. H. Moulden, eds., Plenum Press, New York.

Link, L. E., Jr., 1979, *Thermal Modeling of Battlefield Scene Components*, Waterways Experiment Station, Vicksburg, Miss., Miscellaneous Paper EL-79-5.

Monteith, J. L., G. Szeicz, and P. E. Waggoner, 1965, "The Measurement of Stomatal Resistance in the Field," *J Appl Ecol*, 2:345-355.

Obukhov, A.M., 1946,"Turbulence in an Atmosphere with a Non-Uniform Temperature," *Trudy In-ta Teoret Geofiz, AN SSSR*, (*Works Inst Theor Geophys Acad Sci, USSR*), 1:95-115 (English Translation in *Boundary-Layer Meteorol*, 1971, 2:7-29).

Ochs, G. R., and R. J. Hill, 1985, "Optical-Scintillation Method of Measuring Turbulence Inner Scale," *Appl Opt*, 24:2430-2432.

Oke, T. R., 1978, *Boundary Layer Climates*, Methuen & Co. LTD, London.

Paulson, C. A., 1970, "The Mathematical Representation of Wind Speed and Temperature Profiles in the Unstable Atmospheric Surface Layer," *J Appl Meteorol*, 9:857-861.

Priestley, C. H. B., 1959, *Turbulent Transfer in the Lower Atmosphere*, Univ. of Chicago Press, Chicago, Ill.

Shapiro, R., 1982, "Solar Radiative Flux Calculations from Standard Surface Meteorological Observations," AFGL-TR-82-0039, Air Force Geophysics Laboratory, Hanscom AFB, MA 01731.

Smithsonian Meteorological Tables, 1951, Smithsonian Institution, Washington, DC.

Staley, D. O., and G. M. Jurica, 1972, "Effective Atmospheric Emissivity Under Clear Skies," *J Appl Meteorol*, 11:349-356.

Thom, A. S., 1972, "Momentum, Mass, and Heat Exchange of Vegetation," *Quart J Roy Meteorol Soc*, 98:124-134.

Tofsted, D. H., and J. B. Gillespie, 1986, "Comparing Results from Three Surface Energy Budget Models," *Proc 6th Ann EOSAEL/TWI Conf*, US Army Atmospheric Sciences Laboratory, WSMR, NM, 401-412.

Tofsted, D. H., and H. J. Auvermann, 1991, *Baseline Resolution of Atmosphere Related FADEWS Modeling Issues, Volume 9, Additional Model Improvements*, TR-0302, U.S. Army Atmospheric Sciences Laboratory, White Sands Missile Range, NM 88002-5501.

Wieringa, J., 1980, "A Revaluation of the Kansas Mast Influence on Measurements of Stress and Cup Anemometer Overspeeding," *Boundary-Layer Meteorol*, 18:411-430.

Woolf, H. M., 1968, *On the Computation of Solar Elevation Angles and the Determination of Sunrise and Sunset Times*, National Meteorological Center, Environmental Sciences Services Administration, Hillcrest Heights, MD.

Wyngaard, J. C., 1973, "On Surface-Layer Turbulence," *Workshop on Micrometeorology*, D. A. Haugen, ed., Amer. Meteorol. Soc., Boston, MA.

Yaglom, A. M., 1977, "Comments on Wind and Temperature Flux-Profile Relationships," *Boundary-Layer Meteorol*, 11:89-102.

APPENDIX A

CALCULATIONS INVOLVING SATURATION SPECIFIC HUMIDITY

The specific humidity at a given temperature is found by multiplying the saturation specific humidity (Q_{sat}) by a fraction between zero and one, where this fraction will either be the relative humidity or the moisture coefficients of the ground or vegetation.

Q_{sat} is normally written as a function of pressure, P, and saturation vapor pressure, e_{sat}. The saturation vapor pressure is a function of the temperature.

$$e_{sat} = 6.1078 \times 10^{aT/(b+T)}, \qquad (A-1)$$

where over water a is 7.5 and b is 237.3, while over ice a is 9.5 and b is 265.5.* Q_{sat} is related to e_{sat} and P through the equation

$$Q_{sat} = \frac{0.62\, e_{sat}}{P - 0.38\, e_{sat}}, \qquad (A-2)$$

which is also found in Haurwitz.*

The derivative of Q_{sat} with respect to temperature is a function of the derivative of e_{sat} with respect to temperature:

$$\frac{de_{sat}}{dT} = \ell n(10)\, \frac{a\, b}{(b+T)^2}\, e_{sat}. \qquad (A-3)$$

Thus

$$\frac{dQ_{sat}}{dT} = \ell n(10)\, \frac{a\, b}{(b+T)^2} \left\{ \frac{1}{1 - 0.38\, e_{sat}/P} \right\} Q_{sat}. \qquad (A-4)$$

This result was found through taking the derivative of Q_{sat} in terms of de_{sat}/dT and finding de_{sat}/dT through taking the derivative of $\ln e_{sat} = \ln(10) f(T)$ and solving for de_{sat}/dT.

Pressure is treated as constant with temperature since it is an input dependent on synoptic events rather than on the temperatures treated within the model. The derivative of Q_{sat} with respect to temperature is thus only a function of e_{sat}.

---

*Haurwitz, B., 1941, *Dynamic Meteorology*, McGraw Hill, New York, pp. 8-10.

APPENDIX B

CONSIDERATION OF NOCTURNAL TEMPERATURE GRADIENT STRUCTURES

1. OVERVIEW

Surface energy budget methodologies, combined with flux-profile equations, can be used to estimate the vertical temperature structure of the surface boundary layer from data observed at a single height during the day. However, at night, the governing equations in this method often fail as the critical Richardson number is surpassed (Hansen, 1977). Under these conditions, gravity waves propagating within the inversion layer are crucial in understanding temporal fluctuations of temperature gradient strength.

In this appendix, a model is proposed to characterize the break frequencies of these wave modes. In this model waves are considered to reflect at both the surface and close to the top of the inversion. Also, the vertical gradient of horizontal wind and the second derivative of temperature are treated as being constant with height. The vertical wavelength is considered to be an integral fraction of the inversion height, and the horizontal wavelength is considered to be 7.5 times the depth of the inversion layer.

Model predictions of frequency modes at 0.210, 0.109, and 0.074 cycles per minute (cyc/min), and corresponding break frequencies of 0.128, 0.034, and 0.011 cyc/min appear to be closely matched to test data values.

2. INTRODUCTION

Over the years many studies have treated the problem of strong stability conditions within the surface layer atmosphere. But the nocturnal problem has continued to present theoretical difficulties. In particular, the application of flux profile parameterizations does not hold during highly stable periods. These parameterizations depend on a fully turbulent atmosphere for their underlying theoretical basis. But at night, calm periods occur when turbulent mixing is highly damped.

In the absence of the flux-profile parameterizations of stable vertical atmospheric structure, some other model must be postulated. As evidenced by equation (61) in the main section of this report, the flux-profile technique cannot obtain a valid solution when the temperature inversion strength impedes vertical mixing of air.

As was discussed, the quick fix to the problem was to limit the computation of u_* to some minimum value. In this way the resulting algorithm always obtains a positive value for the Obukhov length. However, this does not ensure a valid estimation of the vertical structure of the temperature profile. Perhaps this is because the vertical temperature profile is relatively independent of the flux-profile forms under strong inversion conditions. This is the thesis of this section.

When the predominant processes governing the vertical structures of the main parameters within the surface layer are not due to wind driven mixing, there is no readily available theory to gain predictive insight into these structures. An alternative driving mechanism must therefore be sought. It is hypothesized that there are two driving mechanisms: the radiative flux at the surface that is cooling the near surface atmosphere, and standing gravity waves within the boundary layer. The gravity waves so produced tend to gain energy exponentially due to the nonlinear nature of the governing wave equations. Then, since each wave is subject to a turbulent breakdown and since this breakdown has a characteristic time for each wave, the dynamic variability of vertical temperature gradients with time may be explained by periodic mixing episodes corresponding to gravity wave breakdown.

It is hoped that once the temporal structure of the vertical temperature gradient is understood, then the results can be coupled to models indicating the time variability of the flow of turbulent energy to the surface and the dissipation. The knowledge of the energy flow should help in the calculation of the parameters u_*, θ_*, and L.

3. ENERGY BALANCE CONSIDERATIONS

Following the traditional approach to the computation of u_* and L, the nocturnal energy budget is divided into components related to longwave radiative, conductive, and convective fluxes. Since in this analysis we are considering only the most stable atmospheric states, we can safely assume the radiative and conductive fluxes will be the dominant drivers in the energy budget. Rewriting equation (3),

$$R_{L_{g\uparrow}} + H_{S_g} + LE_g + G = R_{L_{g\downarrow}} \quad . \qquad (B-1)$$

In this model the only means of cooling the air near the surface is through the sensible heat flux, but under quiescent conditions it may be that radiative exchange of energy with the surface will cause cooling of the air near the surface. This cooling will depend on numerous factors beyond the scope of this section. However, these additional factors may play key roles in the stable boundary layer problem. Such factors include, but may not be limited to, radiative flux divergence in the stable layer, mechanisms for generating the nocturnal jet flow, drainage winds, and vertical stratification of moisture in the stable layer.

4. THE CRITICAL RICHARDSON NUMBER

At night Dyer (1974) finds

$$\psi_h = \psi_m = \psi = -\beta \frac{z}{L} \quad , \qquad (B-2)$$

as pointed out in the main text. However, Hansen (1977) also indicates the choice of the critical value of the gradient Richardson number is related to β through

$$\beta = 1/R_{i_{crit}} \quad . \qquad (B-3)$$

This critical value is related to the value beyond which turbulent mixing is thought to be damped. Note that this condition is the finding of the analysis in the main text leading to condition (67). Accordingly,

$$R_i = gz(\theta_z - \theta_e)/(\theta_z u^2),$$

from the analysis in the main text, since when R_i reaches its critical value condition (67) will be met. Another way of expressing this equation is

$$R_i = \frac{g T_*}{u_* \theta_z} \frac{z}{u},$$

where T_* is the scaling temperature (Hoffert and Storch, 1979), given by

$$T_* = \frac{k(\theta_z - \theta_e)}{\ell n(\zeta) - \psi},$$

and u_* is the friction velocity given by

$$u_* = \frac{k u}{\ell n(\zeta) - \psi}.$$

Assuming T_* and u_* can both be determined, according to the flux-profile theory they are considered constant over the surface layer. Due to this relationship, R_i is a function of height. Also we can see that since u is zero at $z = z_0$, R_i is infinite at zero height and decreases thereafter. We could therefore expect, even under the limitations of the flux-profile method, that there is some height above which mechanical turbulence exists. The question that remains is how to treat the intervening layer.

In answering this question the critical Richardson number is a valuable measure of the stability of the stable nocturnal boundary layer, and a study of turbulence formation in this layer naturally arrives at an estimation of this parameter. Such a study is performed in the next section with the help of a mathematical construct called a turbulence rotor.

5. A TURBULENCE ROTOR

We can gain further insight into the cutoff of convective fluxes and determine a theoretical value for the critical gradient Richardson number if we model a single rotor of turbulence within the flow. Consider a portion of the general flow of air above the surface. Within a certain small height interval, the flow can be described by average vertical gradients of windspeed and temperature. It is postulated that a parcel of air can become turbulent if it becomes disconnected from the general flow and begins to roll over (assuming this disconnection is through the addition of minimal startup energy). Assuming random small scale turbulent energy exists throughout the flow, such a parcel is always able to arise spontaneously from within the flow.

A further postulation is that the simplest such starter parcel would be shaped like a cylinder.* Its time of existence would be short: drag forces drawing it back into the flow in time. But during its existence it would decrease the vertical gradients of temperature and momentum through mixing of the air at different temperatures and velocities at its upper and lower halves. Figure B-1 shows the model for the hypothesized cylinder at the time of its detachment from the flow.

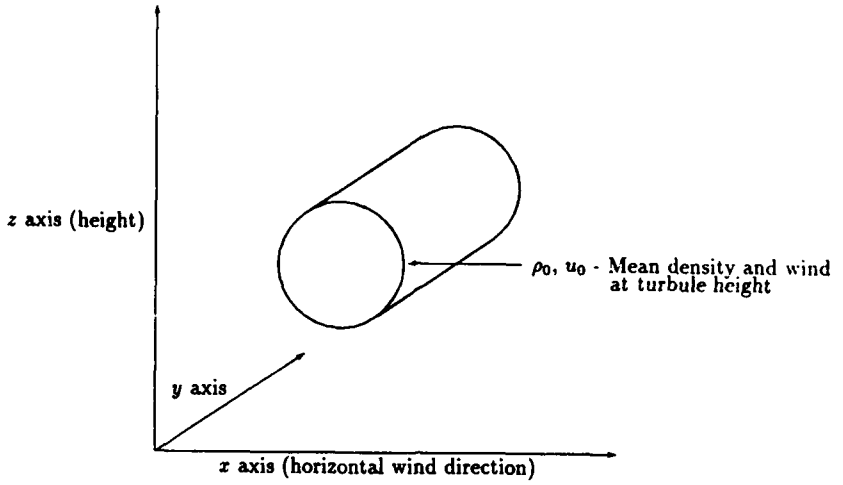

Figure B-1. Vertical cross sections of temperature and wind relative to a turbulence cylinder.

At disconnect time, two competing factors are influencing the cylinder: the rotational kinetic energy possessed by the cylinder that causes it to roll and the negative potential energy that tends to prevent it from rolling. The first of these may be defined by computing $\tilde{L}$, the cylinder's angular momentum, as

$$\tilde{L} = \int_M dm\, r_{\parallel z}\, u_z, \qquad (B-4)$$

where M is the mass of the cylinder, dm is a differential mass element, $r_{\parallel z} = r\sin(\varpi)$ is the vertical distance away from the center of the cylinder, and u_z is the horizontal windspeed at height $r_{\parallel z}$. (See figure B-2 for r and ϖ definitions.)

Then, with ρ_0 the air density at the height of the center of the cylinder, u_0 the windspeed at that height, and assuming $\dot{\rho}$ and $\dot{u}$ (the vertical derivatives of density and horizontal windspeed across the cylinder) are constant, we have

$$u_z = u_0 + \dot{u}\, r\sin(\varpi),$$

*Such structures were observed in experiments where a collimated HeNe laser was propagated through a 2000 m path of air on a calm night. In most cases these turbulent cylinders or spheres appeared to 'roll' through the illuminated surface where the laser pattern was intercepted.

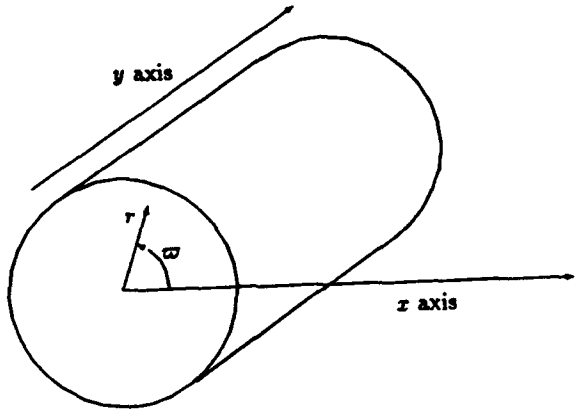

Figure B-2. Definitions of radius (r), angle (ϖ), and width (y) of a turbulence cylinder.

$$dm = \rho\, dV = \rho\, r\, dr\, d\varpi\, dy,$$

$$\rho = \rho_0 + \dot{\rho}\, r \sin(\varpi),$$

$$\dot{\rho} = d\rho/dz,$$

$$\dot{u} = du/dz.$$

These approximations become exact as the vertical size of the cylinder approaches zero. Also, there should be no confusion between this notation and the standard use of the over-dot as a time derivative since time derivatives are not explicitly made in this derivation.

Equation (B-4) can now be rewritten

$$\tilde{L} = \int_0^Y \int_0^{2\pi} \int_0^R \{(\rho_0 + \dot{\rho}\, r \sin(\varpi))\, r\, dr\, d\varpi\, dy\}\{r \sin(\varpi)\}\{u_0 + \dot{u}\, r \sin(\varpi)\}$$

$$= (\rho_0 \dot{u} + \dot{\rho}\, u_0)\frac{V r^2}{4} \quad , \qquad (B-5)$$

where V is the volume of the cylinder. The three quantities within brackets inside the integral correspond to the same three quantities in equation (B-4).

From the angular momentum, the rotational kinetic energy can be calculated.

$$E_K = \frac{\tilde{L}^2}{2I} \quad ,$$

where I is the rotational inertia. For a cylinder,

$$I = \frac{\rho V r^2}{2} \quad ,$$

so that

$$E_K = \left\{ (\rho_0 \dot{u} + \dot{\rho} u_0) \frac{V r^2}{4} \right\}^2 / \rho_0 V r^2 \quad . \qquad (B-6)$$

The next quantity to be determined is the rotational potential energy to be overcome. To compute this quantity the torque must be evaluated. The torque induced by rotating the cylinder in the presence of a density gradient can be defined relative to an arbitrary angle ϑ, the angle of rotation from the equilibrium position. Computing the torque involves another integration over the cylinder's volume.

$$\vec{\tau} = \int_V \vec{r} \times d\vec{F}. \qquad (B-7)$$

Based on the geometry of figure B-2, the torque can be defined as $\tau \hat{j} = \vec{\tau}$, where $\hat{j}$ is the unit vector in the y direction. In simplifying the notation, the torque's y-component will hereafter be referred to as the torque, τ. The right-hand side of equation (B-7) can be calculated using the figure B-2 definition of $\vec{r}$, and

$$d\vec{F} = -d\rho \, g \, dV \, \hat{k},$$

where $d\rho$ is the density difference between the volume element's equilibrium level and its current level, and $\hat{k}$ is the unit vector in the $+z$ direction. Since density is assumed to vary linearly with height,

$$d\rho = \dot{\rho} r (\sin(\varpi + \vartheta) - \sin(\varpi)).$$

$$\tau = \int_0^Y \int_0^{2\pi} \int_0^R r \cos(\varpi + \vartheta) \, \{ -\dot{\rho} r (\sin(\varpi + \vartheta) - \sin(\varpi)) \, g \, r \, dr \, d\varpi \, dy \}$$

$$= \dot{\rho} g V \sin(\vartheta) \frac{r^2}{4}. \qquad (B-8)$$

Assume that the cylinder can be considered a true turbule if it can rotate through π radians (it can turn over). The amount of potential energy that must be overcome is found by integrating the torque through π radians.

$$E_P = \int_0^{\pi} \tau \, d\vartheta = 2 \dot{\rho} g V \frac{r^2}{4} \quad .$$

Setting the amount of potential energy to be overcome equal to the kinetic energy available, an equation for the necessary $\dot{u}$ is developed.

$$0 = \dot{u}^2 + \left(\frac{2 u_0 \dot{\rho}}{\rho_0} \right) \dot{u} + \left(\frac{u_0^2 \dot{\rho}^2}{\rho_0^2} - \frac{8 g \dot{\rho}}{\rho_0} \right). \qquad (B-9)$$

Solving for $\dot{u}$,

$$\dot{u} = \sqrt{8gQ} - u_0 Q, \qquad (B-10)$$

where

$$Q = \frac{\dot{\rho}}{\rho_0}. \qquad (B-11)$$

From this development, $\dot{u}$ defines the minimum positive gradient of windspeed necessary for turbulence to be initiated (ignoring drag effects that might be present over the first π radians). Further, since

$$\frac{\dot{\rho}}{\rho_0} = -\frac{1}{\theta}\frac{d\theta}{dz},$$

(ignoring vertical pressure gradient effects in a highly stable atmosphere), therefore,

$$\frac{du}{dz} = \sqrt{\frac{8g}{\theta}\frac{d\theta}{dz}} + \frac{u}{\theta}\frac{d\theta}{dz} \quad , \qquad (B-12)$$

where $g = 9.8$ m/s^2.

To simplify the above expression, consider the following example: In a strongly stable atmosphere let $z = 2$ m, $\theta = 290$ K, $u = 2$ m/s, and $d\theta/dz = 0.5$ K/m. Then,

$$\frac{du}{dz} = 0.368s^{-1} + 0.00345s^{-1}.$$

Clearly, the first term is the most important, and if the second term also becomes significant because of higher windspeeds, the flux-profile methods will not fail. Therefore only the first term needs to be retained.

Therefore, keeping only the first term on the right, squaring what remains of equation (B-12), and moving terms result in

$$\frac{1}{8} > \left\{ \frac{g}{\theta}\frac{d\theta}{dz} \Big/ \left(\frac{du}{dz}\right)^2 \right\} \quad , \qquad (B-13)$$

where the $>$ sign is introduced to indicate that the condition is necessary for turbulence. But the term on the right is the same equation given by Hansen for the gradient Richardson number, implying a critical value under very stable conditions of $\frac{1}{8}$, and thus β equals 8.

This result corresponds well with the conclusions of Oke (1970) and McVehil (1964) that turbulence drops sharply around Richardson numbers of 0.1 and 0.08, respectively. Since 0.125 is an upper limit according to the theory developed here, test data at lower stabilities will indicate lower effective critical values (through equation (B-10)) in accord with Oke and McVehil. But this result does not compare well with the conclusions of other researchers such as Webb (1970) and Businger *et al.* (1971), who have found critical Richardson numbers around 0.20, though there is no complete agreement on this subject (see particularly Yaglom (1977) and Hansen (1977)).

To understand the discrepancy between equation (B-13) and these other findings, first consider that the arguments addressed thus far have dealt only with turbulence arising from the mean flow characteristics. Since turbulence is commonly observed at higher Richardson numbers, other sources of turbulence must exist that provide turbulent energy between the general flow cutoff value commonly understood to be near 0.2.

One such source of turbulence appears to come from wind interaction with roughness elements at the surface. We can, in fact, argue for such surface based turbulence on similarity theory grounds.

Assuming that the windspeed and temperature profiles are similar (as similarity theory maintains), the ratio of the gradients of temperature and wind should be equal regardless of height above the surface at night. According to Dyer, similarity theory expresses nocturnal gradients of wind and temperature as

$$\frac{du}{dz} = \frac{u_*}{kz}\left(1 + \beta\frac{z}{L}\right) \qquad (B-14)$$

$$\frac{d\theta}{dz} = \frac{T_*}{kz}\left(1 + \beta\frac{z}{L}\right). \qquad (B-15)$$

Therefore, equation (B-13) can be reexpressed as

$$\frac{\theta}{g}\frac{u_*^2}{kT_*}\left(\frac{1}{z} + \frac{\beta}{L}\right) > 8 \quad . \qquad (B-16)$$

Assuming that meaningful values of θ_*, u_*, and L can be drawn from profile data, there must be some level, z, low enough that the $1/z$ term in equation (B-16) is dominant, and the inequality can be satisfied. Turbulence elements produced between the zero plane and this level will then generate turbulence that can propagate upward into the turbulence suppressed region. This effect, however, will only influence near-surface conditions, which would not allow for transfer of energy between the base and top of the inversion layer.

A second source of continuing turbulence may be remaining energy from the unstable boundary layer in existence before sunset. As noted by Arya (1972), preexisting turbulence must be considered when turbulence at Richardson numbers of 0.25 or more is observed. However, even this turbulence will rise to the top of the stable layer with time, and thus does not provide a mechanism for maintaining turbulent energy exchange with the surface throughout the night.

6. GRAVITY WAVES

A third source for turbulence is caused by the breakdown of waves, which allows transport of turbulent energy to the surface throughout the stable period. These waves are characterized by periodic breakdowns that disturb the surface layer atmosphere.

Kelvin-Helmholtz waves (Atlas, 1970) and other types of gravity waves (Davis, 1976) produced throughout the inversion layer grow and periodically break, producing turbulent episodes during an otherwise calm evening. These periods often occur as dips or spikes of

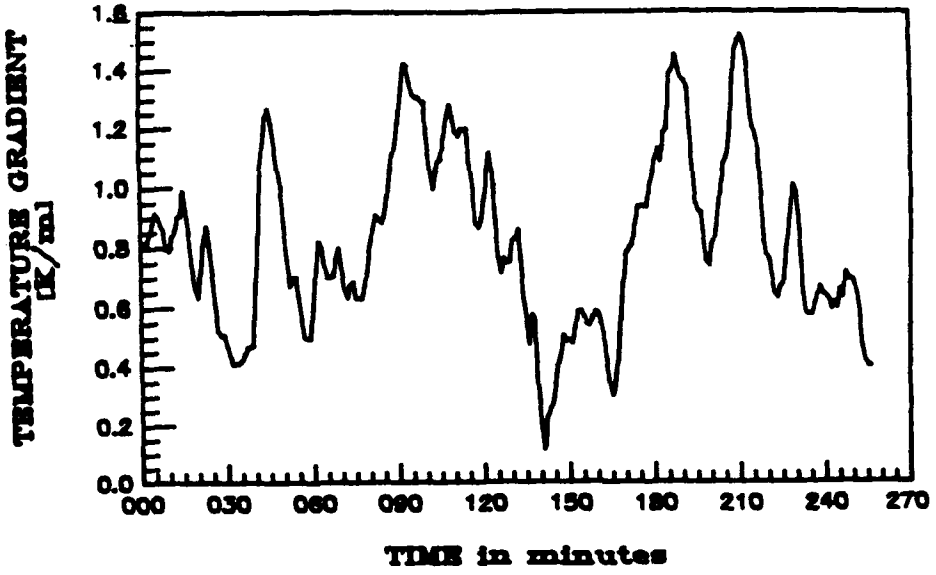

Figure B-3. Vertical temperature gradient at 2 m above ground level as a function of time. This is period 2 of data taken at WSMR, NM, on the night of 8 Sep 1984.

turbulence throughout an evening (for example, see Kunkel and Walters' (1983) figures 1 through 3). Similarly, the time structure of the temperature gradient does not vary smoothly during the night, as might otherwise be implied by Wyngaard's study (1975). These waves are manifested in periodic increases and decreases in the vertical temperature gradient (figure B-3).

Some of the key findings from studies conducted to understand gravity wave behavior are presented in this section. A general treatise on gravity waves is available in Beer (1974), where the elemental energy and momentum conservation equations are used to derive several wave equations under different atmospheric conditions. A modified version of Beer's method for an inversion layer case will be developed here. Beer notes that gravity waves are reflected at a level where their fundamental frequency matches the Brunt-Viasala frequency. This means that all waves propagating within the surface layer will remain within this layer, reflecting at the ground as well as near the top of the inversion.

However, a fraction of these waves is never reflected since they are absorbed before reaching the inversion height. The height of absorption is characterized by the condition (Booker, 1967)

$$\omega - \kappa_x u_a = 0 \quad , \qquad (B-17)$$

where ω is the radial wave frequency, κ_x is the horizontal wave number, and u_a is the windspeed at the absorption height. The left-hand side of the equation is also called the Doppler velocity, Ω. Thus, absorption occurs at the level where the Doppler velocity vanishes. This covers most short wavelength modes (large wave number) that are absorbed

well below the inversion level. For longer wavelength modes, there is the possibility for tunneling through the potential barrier at the inversion height, but this case is not dealt with. Results obtained by ignoring tunneling are virtually identical to a full analysis, but are mathematically much simpler (Orlanski, 1973).

A rich selection of material is available on the rate of growth of different wavelength modes. Results vary, depending on the density and windspeed vertical structures chosen, but as Lalas and Einaudi (1976) report, the wavelength of the fastest growing mode has been found as being between 7.14 and 7.66 times the depth of the shear layer studied. Davis and Peltier (1976) find a fastest growing wavelength of 6.55 times the depth of the inversion layer. Traditionally, however, the coefficient 7.5 appears most frequently in the literature (Browning, 1971; Miles and Howard, 1964; Goldstein, 1931), and apparently dates back to the works of Rayleigh (1880, 1887). This traditional value was used in this analysis. In our case the characteristic shear layer depth is the depth of the inversion layer, Z_i, assumed to range between 100 and 400 m (Arya, 1981). Corresponding fastest growing mode wave numbers are

$$\kappa_x = \frac{2\pi}{7.5 Z_i} \quad . \qquad (B-18)$$

6.1 Derivation of the Wave Equation

The derivation of the wave equation governing surface layer propagating gravity waves closely follows a procedure described by Beer (1974). In his exposition, Beer manipulated the equations of motion in x and z directions, x being along the direction of the wind and z being the upward direction. He also included the energy conservation and mass continuity equations, to obtain four equations similar to those of equation set (B-19).

$$-i\kappa_x g H\left(\frac{P'}{P_0}\right) + u'_x \frac{du_x}{dz} + \hat{Q}u'_x = 0 \qquad \text{(B-19a)}$$

$$g\left(\frac{\rho'}{\rho_0} - \frac{P'}{P_0}\right) + gH\frac{d}{dz}\left(\frac{P'}{P_0}\right) + \hat{Q}u'_z = 0 \qquad \text{(B-19b)}$$

$$\gamma\chi - \frac{u'_z}{H} + \hat{Q}\left(\frac{P'}{P_0}\right) = 0 \qquad \text{(B-19c)}$$

$$\chi - \frac{u'_z}{H}(1+\dot{H}) + \hat{Q}\left(\frac{\rho'}{\rho_0}\right) = 0 \quad , \qquad \text{(B-19d)}$$

where $i = \sqrt{-1}$ is the imaginary root, H is the atmospheric density scale height ($H \approx 8000$ m), χ is the wind divergence,

$$\chi = \frac{du'_x}{dx} + \frac{du'_z}{dz} \quad ,$$

$\hat{Q}$ is a linearized operator proportional to the Doppler frequency ($\hat{Q} = i\Omega$), γ is the ratio of specific heats, and the four variables: pressure (P), density (ρ), horizontal windspeed (u_x), and vertical windspeed (u_z), are considered to consist of an average value and a small perturbation (the primed portion). For example

$$u_x = u_{x_0} + u'_x \quad . \qquad (B-20)$$

Equation set (B-19) differs from Beer's set (equations (2.5.1) through (2.5.4)) by the last term on the left-hand side of equation (B-19a). This term accounts for the gradient of horizontal windspeed with height in the surface layer. Beer's analysis results in the following wave equation

$$\frac{d^2W}{dz^2} - \frac{1}{H}\left\{1 + \frac{K_x^2 c^2}{(K_x^2 c^2 - \Omega^2)}\frac{dH}{dz}\right\}\frac{dW}{dz} + \left\{\frac{K_x^2}{\Omega^2}\left((\gamma-1)\frac{g^2}{c^2}\frac{g}{H}\frac{dH}{dz}\right) + \frac{\Omega^2}{c^2} - K_x^2 + \frac{K_x^2 c^2}{\gamma H^2 (K_x^2 c^2 - \Omega^2)}\frac{dH}{dz}\right\} W = 0 \qquad (B-21)$$

By using the following substitutions

$$\gamma g H = c^2 \qquad \dot{H} = \frac{dH}{dz} \qquad \ddot{W} = \frac{d^2W}{dz^2}$$
$$\hat{\beta} = K_x^2 c^2 \qquad \Gamma = \hat{\beta} - \Omega^2 \qquad \dot{W} = \frac{dW}{dz}$$

equation (B-21) can be rewritten as

$$\ddot{W} - \frac{1}{H}\left(1 + \frac{\hat{\beta}\dot{H}}{\Gamma}\right)\dot{W} + \left\{\frac{\hat{\beta}}{(\Gamma\gamma H)^2}\left(\gamma - 1 + \frac{\hat{\beta}\gamma\dot{H}}{\Gamma}\right) - \frac{\Gamma}{\gamma g H}\right\} W = 0 \quad . \qquad (B-22)$$

6.2 Wave Frequencies and Break Intervals

W represents that portion of the solution for the vertical perturbation velocity u'_z that is dependent on height. In Beer's approach the proposed form for u'_z is

$$u'_z(x,z,t) = W(z)\exp(i(\omega t - K_x x)) \quad , \qquad (B-23a)$$

where

$$W(z) = \overline{Z}\exp(-i K_z z) \qquad (B-23b)$$

$$K_z = \kappa_{z_{real}} + i\kappa_{z_{imaginary}} \quad , \qquad (B-23c)$$

and $\overline{Z}$ is a complex constant. W therefore represents the envelope of the complex phase. This approach assumes the equation of motion is separable. Also, it assumes fixed forms for the vertical temperature and mean windspeed structures.

To find a frequency ω for this form of solution, equation (B-22) can be rewritten as

$$\ddot{W} + D\dot{W} + SW = 0 \quad . \qquad (B-24)$$

Then using equation set (B-23), the wave equation can be broken into two equations, written in terms of real and imaginary parts of the wave number K_z.

$$-\kappa_{z_r}^2 + \kappa_{z_i}^2 + D\kappa_{z_i} + S = 0 \qquad (B-25a)$$

$$2i(\kappa_{z_r}\kappa_{z_i}) - iD\kappa_{z_r} = 0 \quad . \qquad (B-25b)$$

Solving these equations for κ_{z_i} and κ_{z_r}, we find

$$\kappa_{z_i} = \frac{D}{2} \qquad (B-26a)$$

$$\kappa_{z_r} = \sqrt{S + \frac{3}{4}D^2} \quad . \qquad (B-26b)$$

By using the boundary conditions

$$W(0) = W(Z_i) = 0 \quad ,$$

we obtain

$$\kappa_{z_r} = \frac{n\pi}{Z_i} = \sqrt{S + \frac{3}{4}D^2},\ n = 1,2,3\ldots \quad , \qquad (B-27)$$

which is a similar result to that obtained by Davis and Peltier (1976), where standing waves appear below the inversion level.

This discussion can be extended to equation set (B-19) quite readily once a wave equation comparable to equation (B-22) is found. Working through equation set (B-19) with Beer's method results in

$$\ddot{W} + \left\{-\frac{1}{H}\left(1 + \frac{\hat{\beta}\dot{H}}{\Gamma}\right) + \frac{\kappa_x \dot{u}_x}{\Omega}\right\}\dot{W}$$

$$+\left\{\frac{(\hat{\beta} - \kappa_x \dot{u}_x \Omega H\gamma)}{(\Omega H\gamma)^2}\left(\gamma - 1 + \frac{\gamma\hat{\beta}\dot{H}}{\Gamma}\right) - \frac{\Gamma}{\gamma g H}\right\}W = 0 \quad . \qquad (B-28)$$

By inserting the new forms for D and S into equation (B-27), a transcendental equation in ω emerges that can be solved iteratively with the Newton-Raphson method as follows: Set

$$\nu = \frac{n^2\pi^2}{Z_i^2}.$$

From equation (B-27) a function $J(\omega)$ can be used

$$J(\omega) = \frac{3}{4}D^2 + S - \nu = 0 \quad ,$$

whose roots must be found. These roots are determined by selecting some initial value for ω: ω_0. The Newton-Raphson method is then used to determine the root:

$$\omega_{m+1} = \omega_m - J(\omega_m)\Big/\left(\frac{dJ}{d\omega}\right)_{(\omega_m)},$$

where

$$\frac{dJ}{d\omega} = \frac{3D}{2}\frac{dD}{d\omega} + \frac{dS}{d\omega}$$

$$\frac{dD}{d\omega} = -2\frac{\Omega\hat{\beta}\dot{H}}{\Gamma^2 H} - \frac{\kappa_x \dot{u}_{x_0}}{\Omega^2}$$

$$\frac{dS}{d\omega} = 2\frac{\Omega}{\gamma g H} - \frac{\kappa_x \dot{u}_{x_0}\hat{\beta}\dot{H}}{\Gamma^2 H} - (2\hat{\beta} - \kappa_x \dot{u}_{x_0}\gamma H\Omega)\frac{\{(\gamma-1)\Gamma^2 + \gamma\hat{\beta}\dot{H}(\Gamma - \Omega^2)\}}{\Omega^3(\gamma H\Gamma)^2} \quad .$$

Using this method the value of ω can be computed at a given height. In this wave equation, however, the value of ω will vary with height. This characteristic of the wave leads to an interesting paradox: while $\hat{Q}$ was assumed constant with height, ω is a function of height whose gradient is not necessarily small. The resolution to this apparent contradiction is that when the governing equations are reviewed, we find that the terms involving $d\Omega/dz$ are small compared to other factors in the equations. Thus the wave frequencies computed as functions of height will not be significantly in error.

The reason for ω's variation with height comes from the necessity that κ_{z_r} be conserved throughout the depth of the inversion layer. If this were not true, the wave would destructively interfere with itself at every reflection and little wave energy could be built up. The wave frequency therefore changes with height so that κ_{z_r} can be "transported" within the layer, as Whitham (1974) points out in detail.

Following Whitham's arguments further, the wave propagation established when any wave has a frequency that varies with position is inherently unstable. That is, the wave will eventually catastrophically interfere with itself, creating a breaking action similar to that experienced by a wave on the ocean as it approaches the shore. The crest of the wave rises precipitously, and cannot support itself. The nature of the characteristic time of existence of such a wave is a function of the initial differences in phase between the top and the bottom of a wave. Assuming the wave is in phase at the time of its building, it proceeds toward a breakdown at a characteristic time later that Whitham describes as

$$t_B = -1\Big/\frac{d}{dz}\left(\frac{d\omega}{d\kappa_{z_r}}\right). \qquad (B-29)$$

Computationally, this equation can be determined by finding ω for two close values of κ_{z_r} around the solution values for these two terms at some height z. Then, $d\omega/d\kappa_{z_r}$ can be evaluated at a second height $z + dz$ and the derivative computed.

When this procedure was followed for temperature gradient data collected at WSMR in 1984 and compared with the Fourier transform of this data, it was discovered (Tofsted, 1987) that wave frequencies and/or breakdown frequencies were present in the data at around 0.0018, 0.004, 0.008, 0.012, and 0.015 radians/sec (0.017, 0.038, 0.076, 0.115, and 0.143 cycles per minute). As mentioned in the introduction, model predictions were made to determine characteristic wave frequencies for this case. Frequencies of 0.210, 0.109, and 0.074 cycles per minute and corresponding break frequencies of 0.128, 0.034, and 0.011 cyc/min were determined based on the mean temperature, temperature gradient, and windspeed observed during these trials.

This case shows that apparently there is a reasonable connection between the observed data and the predictions. More trials would be necessary to validate this hypothesis. Also, the method does not help in providing any predictive information concerning the expected strength of the gradient and the interference effects between energy released when one wave breaks the buildup of energy at another wavelength.

The source of gravity wave energy apparently is the wind field aloft. Lilly and Klemp (1979) and Peltier and Clark (1979) focus on mountain wave formations, but orographic effects of nearly any degree are probably sufficient to produce waves effects of all wavelengths due to the dispersive nature of gravity waves. In particular, for regions near mountains, lee waves can transport energy downward into the inversion layer where it becomes effectively trapped through conversion into shorter wavelength modes. Once confined, these waves are capable of carrying momentum vertically within the inversion layer without turbulent interaction. As noted by Arya (1981), this wave energy could be the source of continuing turbulence up to Richardson numbers of 0.25, since at the time of wave breaking, energy carried within the waves should convert directly into localized turbulence. Also, in view of dispersion, there should always be background turbulence from energy transfer to shorter wavelength modes. With very short breaking times, these modes continually feed small amounts of turbulent energy into the flow.

Using the gravity wave model one possibility for simulating fluctuations in vertical temperature gradient would be to treat the wave mode effects as independent and allow them to influence the total temperature gradient as a sum of effects. This technique would use an equation of the type

$$\frac{d\theta}{dz} = \sum_i A_i \sin(\omega_i t + \Theta_{\omega_i})\, F(t_{B_i}, \Theta_{B_i}, t) + \overline{\frac{d\theta}{dz}}, \qquad (B-30)$$

where $F(t_{B_i}, t)$ would describe function for the bounding envelope of the building and breaking of the wave, and Θ_{ω_i} and Θ_{B_i} are random phases of the wave and breaking times. Simple functions describing the F function would be sines and cosines or combinations thereof. Similar functions could be developed for C_T^2, C_n^2, and C_v^2. Since the periods of breaking of some of these waves are as little as 5 min, measurements must be taken at least 10 times as fast as this rate and the time scale of the surface energy budget model must be set as fast or faster than this rate. Thus at night the time step should be no more than 30 seconds (when wave phenomena are considered).

7. Approximation of Temperature Gradient

In lieu of a temperature gradient calculation based on gravity wave effects (which is currently in a notional form), an empirical adjustment technique has been developed to improve nocturnal temperature gradient estimates. In this technique the parameter Q_q is used, where

$$Q_q = \sqrt{8\, g\, \dot{\rho}/\rho} - u_z \dot{\rho}/\rho. \qquad (B-31)$$

(Q_q is the right-hand side of equation (B-10). This parameter is then used in the equation

$$X = \min(1.5,\, Q/(du/dz)). \qquad (B-32)$$

The temperature gradient is then adjusted (for non-negative temperature gradients) by the equation

$$\frac{d\theta}{dz} = \frac{d\theta}{dz}(1 - 0.125\,X + 0.375\,X^2). \qquad (B-33)$$

For $X < 1/3$, the maximum difference between this correction and the normal temperature gradient calculation occurs at $X = 1/6$ where the correction factor is $1 - 1/96$. Beyond $X = 1/3$ the correction factor increases to the maximum of 1.5 at $X = 4/3$. This value for X represents a point $1/3$ beyond the $X = 1$ value where the similarity equations fail. This equation therefore induces small underestimating error for $X < 1/3$, but for large X the error between measured and predicted temperature gradient is reduced. Since the correction term is dependent on the variable that influences the ability of turbulent turnover of small turbules as discussed in section 5. of this appendix, the correction thus increases the temperature gradient to compensate for the error induced by setting u_* to a minimum value to avoid negative L values.

LITERATURE CITED IN APPENDIX B

Arya, S. P. S., 1972, "The Critical Condition for the Maintenance of Turbulence in Stratified Flows," *Quart J Roy Meteorol Soc*, 98:264-273.

Arya, S. P. S., 1981, "Parameterizing the Height of the Stable Atmospheric Boundary Layer," *J Appl Meteorol*, 20:1192-1202.

Atlas, D., J. I. Metcalf, J. H. Richter, and E. E. Gossard, 1970, "The Birth of "CAT" and Microscale Turbulence," *J Atmos Sci*, 27:903-913.

Beer, T., 1974, *Atmospheric Waves*, John Wiley & Sons, New York.

Booker, J. R., and F. P. Bretherton, 1967, "The Critical Layer for Internal Gravity Waves in a Shear Flow," *J Fluid Mech*, 27:3:513-539.

Browning, K. A., 1971, "Structure of the Atmosphere in the Vicinity of Large-Amplitude Kelvin-Helmholtz Billows," *Quart J Roy Meteorol Soc*, 97:283-299.

Businger, J. A., J. C. Wyngaard, Y. Izumi, and E. F. Bradley, 1971, "Flux-Profile Relationships in the Atmospheric Surface Layer," *J Atmos Sci*, 28:181-189.

Davis, P. A., and W. R. Peltier, 1976, "Resonant Parallel Shear Instability in the Stably Stratified Planetary Boundary Layer," *J Atmos Sci*, 33:1287-1300.

Dyer, A. J., 1974, "A Review of Flux-Profile Relationships," *Boundary-Layer Meteorol*, 7:363-372.

Goldstein, S., 1931, "On the Stability of Superposed Streams of Fluids of Different Densities," *Proc Roy Soc A*, 132:524-548.

Hansen, F. V., 1977, "The Critical Richardson Number," ECOM-5829, U.S. Army Electronics Command, Fort Monmouth, NJ.

Hoffert, M. I., and J. Storch, 1979, "A Scheme for Computing Surface Fluxes From Mean Flow Observations," *Boundary-Layer Meteorol*, 17:429-442.

Kunkel, K. E., and D. L. Walters, 1983, "Modeling the Diurnal Dependence of the Optical Refractive Index Structure Parameter," *J Geophys Res*, 88(C15):10,999-11,004.

Lalas, D. P., and F. Einaudi, 1976, "On the Characteristics of Gravity Waves Generated by Atmospheric Shear Layers," *J Atmos Sci*, 33:1248-1259.

Lilly, D. K., and J. B. Klemp, 1979, "The Effects of Terrain Shape on Nonlinear Hydrostatic Mountain Waves," *J Fluid Mech*, 95:241-262.

McVehil, G. E., 1964, "Wind and Temperature Profiles Near the Ground in Stable Stratification," *Quart J Roy Meteorol Soc*, 90:136-146.

Miles, J. W., and L. N. Howard, 1964, "Note on a Heterogeneous Shear Flow," *J Fluid Mech*, 20:2:331-336.

Oke, T. R., 1970, "Turbulent Transport Near the Ground in Stable Conditions," *J Appl Meteorol*, 9:778-786.

Orlanski, I., 1973, "Trapeze Instability as a Source of Internal Gravity Waves," *J Atmos Sci*, 30:1007-1016.

Peltier, W. R., and T. L. Clark, 1979, "The Evolution and Stability of Finite-Amplitude Mountain Waves," *J Atmos Sci*, 36:1498-1529.

Rayleigh, Lord, 1880, "On the Stability, or Instability, of Certain Fluid Motions," *Proc Lond Math Soc*, 11:57-70.

Rayleigh, Lord, 1887, "On the Stability, or Instability, of Certain Fluid Motions, II," *Proc Lond Math Soc*, 19:67-74.

Tofsted, D. H., 1987, "A Surface Energy Budget Model for European Weather," *Proc 7th Annual EOSAEL/TWI Conference*, US Army Atmospheric Sciences Laboratory, WSMR, NM, 465-476.

Webb, E. K., 1970, "Profile Relationships: the Log-Linear Range, and Extension to Strong Stability," *Quart J Roy Meteorol Soc*, 96:67-90.

Whitham, G. B., 1974, *Linear and Nonlinear Waves*, John Wiley & Sons, New York.

Wyngaard, J. C., 1975, "Modeling the Planetary Boundary Layer - Extension to the Stable Case," *Boundary-Layer Meteorol*, 9:441-460.

Yaglom, A. M., 1977, "Comments on Wind and Temperature Flux-Profile Relationships," *Boundary-Layer Meteorol*, 11:89-102.

DISTRIBUTION LIST FOR PUBLIC RELEASE

Commandant
U.S. Army Chemical School
ATTN: ATZN-CM-CC (S. Barnes)
Fort McClellan, AL 36205-5020

NASA/Marshall Space Flight Center
Deputy Director
Space Science Laboratory
Atmospheric Sciences Division
ATTN: ES01 (Dr. George H. Fichtl)
Huntsville, AL 35812

NASA/Marshall Space Center
ATTN: Code ES44 (Dale Johnson)
Huntsville, AL 35812

NASA/Marshall Space Flight Center
Atmospheric Sciences Division
ATTN: Code ED-41
Huntsville, AL 35812

Deputy Commander
U.S. Army Strategic Defense Command
ATTN: CSSD-SL-L
Dr. Julius Q. Lilly
P.O. Box 1500
Huntsville, AL 35807-3801

Commander
U.S. Army Missile Command
ATTN: AMSMI-RD-AC-AD
Donald R. Peterson
Redstone Arsenal, AL 35898-5242

Commander
U.S. Army Missile Command
ATTN: AMSMI-RD-AS-SS
Huey F. Anderson
Redstone Arsenal, AL 35898-5253

Commander
U.S. Army Missile Command
ATTN: AMSMI-RD-AS-SS
B. Williams
Redstone Arsenal, AL 35898-5253

Commander
U.S. Army Missile Command
ATTN: AMSMI-RD-DE-SE
Gordon Lill, Jr.
Redstone Arsenal, AL 35898-5245

Commander
U.S. Army Missile Command
Redstone Scientific Information
Center
ATTN: AMSMI-RD-CS-R/Documents
Redstone, Arsenal, AL 35898-5241

Commander
U.S. Army Intelligence Center
and Fort Huachuca
ATTN: ATSI-CDC-C (Mr. Colanto)
Fort Huachuca, AZ 85613-7000

Northrup Corporation
Electronics Systems Division
ATTN: Dr. Richard D. Tooley
2301 West 120th Street, Box 5032
Hawthorne, CA 90251-5032

Commander - Code 3331
Naval Weapons Center
ATTN: Dr. Alexis Shlanta
China Lake, CA 93555

Commander
Pacific Missile Test Center
Geophysics Division
ATTN: Code 3250 (Terry E. Battalino)
Point Mugu, CA 93042-5000

Lockheed Missiles & Space Co., Inc.
Kenneth R. Hardy
Org/91-01 B/255
3251 Hanover Street
Palo Alto, CA 94304-1191

Commander
Naval Ocean Systems Center
ATTN: Code 54 (Dr. Juergen Richter)
San Diego, CA 92152-5000

Meteorologist in Charge
Kwajalein Missile Range
P.O. Box 67
APO San Francisco, CA 96555

U.S. Department of Commerce
Mountain Administration Support
Center
Library, R-51 Technical Reports
325 S. Broadway
Boulder, CO 80303

Dr. Hans J. Liebe
NTIA/ITS S 3
325 S. Broadway
Boulder, CO 80303

NCAR Library Serials
National Center for Atmos Rsch
P.O. Box 3000
Boulder, CO 80307-3000

HQDA
ATTN: DAMI-POI
Washington, DC 20310-1067

Mil Asst for Env Sci Ofc of
The Undersecretary of Defense
for Rsch & Engr/R&AT/E&LS
Pentagon - Room 3D129
Washington, DC 20301-3080

HQDA
DEAN-RMD/Dr. Gomez
Washington, DC 20314

Director
Division of Atmospheric Science
National Science Foundation
ATTN: Dr. Eugene W. Bierly
1800 G. Street, N.W.
Washington, DC 20550

Commander
Space & Naval Warfare System Command
ATTN: PMW-145-1G (LT Painter)
Washington, DC 20362-5100

Commandant
U.S. Army Infantry
ATTN: ATSH-CD-CS-OR
Dr. E. Dutoit
Fort Benning, GA 30905-5090

USAFETAC/DNE
Scott AFB, IL 62225

Air Weather Service
Technical Library - FL4414
Scott AFB, IL 62225-5458

USAFETAC/DNE
ATTN: Mr. Charles Glauber
Scott AFB, IL 62225-5008

Commander
U.S. Army Combined Arms Combat
ATTN: ATZL-CAW (LTC A. Kyle)
Fort Leavenworth, KS 66027-5300

Commander
U.S. Army Space Institute
ATTN: ATZI-SI (Maj Koepsell)
Fort Leavenworth, KS 66027-5300

Commander
U.S. Army Space Institute
ATTN: ATZL-SI-D
Fort Leavenworth, KS 66027-7300

Commander
Phillips Lab
ATTN: PL/LYP (Mr. Chisholm)
Hanscom AFB, MA 01731-5000

Director
Atmospheric Sciences Division
Geophysics Directorate
Phillips Lab
ATTN: Dr. Robert A. McClatchey
Hanscom AFB, MA 01731-5000

Raytheon Company
Dr. Charles M. Sonnenschein
Equipment Division
528 Boston Post Road
Sudbury, MA 01776
Mail Stop 1K9

Director
U.S. Army Materiel Systems
Analysis Activity
ATTN: AMXSY-MP (H. Cohen)
APG, MD 21005-5071

Commander
U.S. Army Chemical Rsch,
Dev & Engr Center
ATTN: SMCCR-OPA (Ronald Pennsyle)
APG, MD 21010-5423

Commander
U.S. Army Chemical Rsch,
Dev & Engr Center
ATTN: SMCCR-RS (Mr. Joseph Vervier)
APG, MD 21010-5423

Commander
U.S. Army Chemical Rsch,
Dev & Engr Center
ATTN: SMCCR-MUC (Mr. A. Van De Wal)
APG, MD 21010-5423

Director
U.S. Army Materiel Systems
Analysis Activity
ATTN: AMXSY-AT (Mr. Fred Campbell)
APG, MD 21005-5071

Director
U.S. Army Materiel Systems
Analysis Activity
ATTN: AMXSY-CR (Robert N. Marchetti)
APG, MD 21005-5071

Director
U.S. Army Materiel Systems
Analysis Activity
ATTN: AMXSY-CS (Mr. Brad W. Bradley)
APG, MD 21005-5071

Director
U.S. Army Research Laboratory
ATTN: AMSRL-D
2800 Powder Mill Road
Adelphi, MD 20783

Director
U.S. Army Research Laboratory
ATTN: AMSRL-OP-CI-A
(Technical Publishing)
2800 Powder Mill Road
Adelphi, MD 20783

Director
U.S. Army Research Laboratory
ATTN: AMSRL-OP-CI-AD, Record Copy
2800 Powder Mill Road
Adelphi, MD 20783

Director
U.S. Army Research Laboratory
ATTN: AMSRL-SS-SH
Dr. Z.G. Sztankay
2800 Powder Mill Road
Adelphi, MD 20783

National Security Agency
ATTN: W21 (Dr. Longbothum)
9800 Savage Road
Ft George G. Meade, MD 20755-6000

U. S. Army Space Technology
and Research Office
ATTN: Brenda Brathwaite
5321 Riggs Road
Gaithersburg, MD 20882

OIC-NAVSWC
Technical Library (Code E-232)
Silver Springs, MD 20903-5000

The Environmental Research
Institute of Michigan
ATTN: IRIA Library
P.O. Box 134001
Ann Arbor, MI 48113-4001

Commander
U.S. Army Research Office
ATTN: DRXRO-GS (Dr. W.A. Flood)
P.O. Box 12211
Research Triangle Park, NC 27709

Dr. Jerry Davis
North Carolina State University
Department of Marine, Earth, &
Atmospheric Sciences
P.O. Box 8208
Raleigh, NC 27650-8208

Commander
U. S. Army CECRL
ATTN: CECRL-RG (Dr. H. S. Boyne)
Hanover, NH 03755-1290

Commanding Officer
U.S. Army ARDEC
ATTN: SMCAR-IMI-I, Bldg 59
Dover, NJ 07806-5000

U.S. Army Communications-Electronics
Command EW/RSTA Directorate
ATTN: AMSEL-RD-EW-OP
Fort Monmouth, NJ 07703-5206

Commander
U.S. Army Satellite Comm Agency
ATTN: DRCPM-SC-3
Fort Monmouth, NJ 07703-5303

6585th TG (AFSC)
ATTN: RX (CPT Stein)
Holloman AFB, NM 88330

Department of the Air Force
OL/A 2nd Weather Squadron (MAC)
Holloman AFB, NM 88330-5000

PL/WE
Kirtland AFB, NM 87118-6008

Director
U.S. Army TRADOC Analysis Command
ATTN: ATRC-WSS-R
White Sands Missile Range, NM 88002

USAF Rome Laboratory Technical
Library, FL2810 Corridor W, Site 262,
RL//SUL (DOCUMENTS LIBRARY)
26 Electronics Parkway, Bldg 106
Griffiss AFB, NY 13441-4514

AFMC/DOW
Wright-Patterson AFB, OH 0334-5000

Commandant
U.S. Army Field Artillery School
ATTN: ATSF-TSM-TA
Mr. Charles Taylor
Fort Sill, OK 73503-5600

Commander
Naval Air Development Center
ATTN: Al Salik (Code 5012)
Warminister, PA 18974

Commander
U.S. Army Dugway Proving Ground
ATTN: STEDP-MT-DA-M
Mr. Paul Carlson
Dugway, UT 84022

Commander
U.S. Army Dugway Proving Ground
ATTN: STEDP-MT-DA-L
Dugway, UT 84022

Commander
U.S. Army Dugway Proving Ground
ATTN: STEDP-MT-M (Mr. Bowers)
Dugway, UT 84022-5000

Defense Technical Information Center
ATTN: DTIC-FDAC (2)
Cameron Station
Alexandria, VA 22314

Commanding Officer
U.S. Army Foreign Science &
Technology Center
ATTN: CM
220 7th Street, NE
Charlottesville, VA 22901-5396

Naval Surface Weapons Center
Code G63
Dahlgren, VA 22448-5000

Commander
U.S. Army OEC
ATTN: CSTE-EFS
Park Center IV
4501 Ford Ave
Alexandria, VA 22302-1458

Commander and Director
U.S. Army Corps of Engineers
Engineer Topographics Laboratory
ATTN: ETL-GS-LB
Fort Belvoir, VA 22060

TAC/DOWP
Langley AFB, VA 23665-5524

U.S. Army Topo Engineering Center
ATTN: CETEC-ZC
Fort Belvoir, VA 22060-5546

Commander
Logistics Center
ATTN: ATCL-CE
Fort Lee, VA 23801-6000

Commander
USATRADOC
ATTN: ATCD-FA
Fort Monroe, VA 23651-5170

Science and Technology
101 Research Drive
Hampton, VA 23666-1340

Commander
U.S. Army Nuclear & Cml Agency
ATTN: MONA-ZB Bldg 2073
Springfield, VA 22150-3198